5-2022

Exploring DNA Compaction Via Bacillus Subtilis ParB Protein by Single Molecule Investigation

Miranda L. Molina
The University of Texas Rio Grande Valley

EXPLORING DNA COMPACTION VIA BACILLUS SUBTILIS PARB PROTEIN BY SINGLE MOLECULE INVESTIGATION

A Thesis

by

MIRANDA L. MOLINA

Submitted in Partial Fulfillment of the

Requirements for the Degree of

MASTER OF SCIENCE

Major Subject: Biochemistry and Molecular Biology

The University of Texas Rio Grande Valley

May 2022

EXPLORING DNA COMPACTION VIA BACILLUS SUBTILIS PARB PROTEIN BY SINGLE MOLECULE INVESTIGATION

A Thesis

by

MIRANDA L. MOLINA

COMMITTEE MEMBERS

Dr. HyeongJun Kim

Chair of Committee

Dr. Ahmed Touhami

Committee Member

Dr. Michael Persans

Committee Member

May 2022

ABSTRACT

Molina, Miranda L., Exploring DNA Compaction via Bacillus Subtilis ParB Protein by Single Molecule Investigation. Master of Science (MS), May, 2022, 78 pp., 4 tables, 22 figures, references, 44 titles.

Faithful chromosome segregation involves ParB, a DNA-binding and compacting protein that specifically recognizes *parS* DNA sites near the replication origin. ParB spreads 10-20 kb from *parS* sites, which recruitments additional ParB molecules to neighboring DNA, forming higher-order nucleoprotein complexes. ParB is also a novel CTPase enzyme and hydrolyses CTP to self-dimerization and create a clamp that slides along DNA. To understand the roles of CTP in *Bacillus subtilis* ParB (BsParB), we purified wild type ParB (BsParB (WT)) and recombinant ParB (BsParB(R80A)) mutant. BsParB(R80A) was known to prevent CTP binding and not compact DNA. Proteins N- and C-terminally appended with a lysine-cysteine-lysine (KCK) tag were tested. We performed single-molecule DNA flow-stretching experiments both in the absence and presence of CTP. Both CTP binding and CTP hydrolysis impacts ParB-mediated DNA compaction, with *parS* sites modulating compaction rates, while BsParB(R80A) could compact DNA in a CTP-dependent manner. The KCK tag influenced DNA compaction.

DEDICATION

The completion of my master's studies would not have been possible without the love and support of my family and friends. I thank my mother, Olga Molina, my father, Jerry Molina, and my brothers Joseph Molina and Aaron Alaniz, for supporting me in this endeavor.

ACKNOWLEDGMENTS

I will always be grateful to Dr. HyeongJun Kim, chair of my thesis committee, for all of the mentoring and advice over the course of my program.

TABLE OF CONTENTS

LIST OF TABLES

Page

LIST OF FIGURES

Page

CHAPTER I

INTRODUCTION

Statement of the Problem

The ParB protein is a member of the ParABS partition system in bacteria that is involved with faithful chromosome segregation. The Type I partitioning system is the most prevalent partitioning system present on most bacterial plasmids and all chromosomes that have a Par system, including *B. subtilis* (14). The ParABS system consists of ParA, a Walker type ATPase, the DNA-binding protein and novel CTPase ParB, and a *parS* site located near the origin of replication (6). Faithful chromosome segregation is essential to life since bacteria must condense the entire genome into a cell and accurately segregate the condensed genome during DNA replication and cellular division.

It is known that ParB binds to *parS* sites with a high affinity (5) and to non-specific DNA with a low affinity (11, 33, 39) ParB also has the ability to condense DNA into large nucleoprotein complexes (6, 26) and is thought to involve one-dimensional lateral spreading along the DNA (28, 31) as well as three-dimensional DNA bridging between ParB molecules located on distant DNA segments (7, 11, 15, 33, 37, 39). ParB is also required to recruit Structural Maintenance of Chromosomes (SMC) protein (1) and to recruit ParA to a

ParB-*parS* partition complex (11, 14, 21, 23, 29). What is not known yet is how CTP interacts with and modulates the ParB DNA-binding and compacting in relation to the *parS* site and non-specific DNA within the chromosome, as well as the ParA recruiting abilities of ParB in the ParABS system through cytidine triphosphate (CTP) binding and CTP hydrolysis.

Statement of the Purpose

The purpose of this thesis is to elucidate the effect of the nucleoside triphosphate cytidine triphosphate (CTP) on the activities of the novel CTPase and DNA-binding protein *Bacillus subtilis* ParB (BsParB). We are comparing the effect of adding a hydrolysable CTP and non-hydrolysable analog CTPγS to both the wildtype ParB (BsParB (WT) and a spreading-defective and CTP-binding mutant R80A (BsParB(R80A)) (2, 36). To achieve the aim, we are utilizing single-molecule flow-stretching assay to measure DNA compaction rates by BsParB under different nucleotide status as a main tool.

CHAPTER II

REVIEW OF THE LITERATURE

Bacillus subtilis ParB (BsParB) is involved in the ParABS system and SMC recruitment

The ParABS system is a Type I chromosomal partitioning system found in prokaryotes and is the most common partitioning system type that is found on most bacterial plasmid DNA and all chromosomal DNA that has a partitioning system (10). The ParABS system consists of ParA, a Walker-type ATPase, the DNA-binding protein and novel CTPase ParB, and a *parS* site, a 16-bp palindromic sequence of 5'-TGTTNCACGTGAAACA-3', which is located near the origin of replication (6, 24). In the *B. subtilis* genome, there are eight *parS* sites (7, 39). The ParB protein consists of an N-terminal domain (NTD) involved in protein–protein interactions, a central DNA binding domain (DBD) and a C-terminal domain (CTD) that facilitates ParB dimerization and non-specific DNA binding (37). There is much evidence that suggests that the NTD and the DBD can engage in dimerization and even tetramerization, and the CTD can also dimerize with the CTD of another ParB protein (8, 13, 22, 34, 36).

Previous research has shown that ParB binds to *parS* sites with a high affinity (5) and to non-specific DNA with a low affinity (11, 33, 39). *B. subtilis* ParB is also able to bind to specific *parS*-containing DNA as well as non-specific DNA in an independent manner but likely

synergistic manner (13, 39). ParB also has the ability to condense DNA into large nucleoprotein complexes that span thousands of base pairs (6, 15, 26) and is thought to involve one-dimensional lateral spreading along the DNA that is 10-20 kbp away from the *parS* site (28, 31); however, the one-dimensional spreading model is strongly indicated to not be the main mechanism of ParB propagation since diffusion of proteins along DNA may be limited to 100bp from the *parS* site, which is much smaller than the 10kbp spreading observed (16). There is as well a three-dimensional DNA bridging activity between ParB molecules located on distant DNA segments (7, 11, 15, 33, 37, 39). The ParB-*parS* nucleoprotein complexes are likely the result of both protein-protein interactions as well the non-specific protein DNA interactions where a single molecule of DNA is trapped in loops (7, 39). One model that attempts to describe how ParB binds to *parS* DNA is the "nucleation and caging" model for the assembly of the ParABS partitioning complex comprised of ParB forming a dynamic and fluctuating lattice structure around DNA *parS* sites (33).

In cellular conditions, ParB exists in a monomeric and dimeric state in the absence of DNA (39), with ParB dimers likely dimerizing via their CTD (37). Upwards of 90% of ParB dimers are constrained to an active ParB-*parS* (ParBS) partition complex, which indicates that there is a very high concentration of ParB within the partition complex in the 100 μM range (33). The specific yet transient nature of the ParBS partitioning complex is not well characterized. There is the question of how a relatively limited amount of protein in the cell (15) can localize to so few *parS* sites (eight) on the genome, but DNA-binding and compaction do not require the presence of a *parS* site (7, 15; 39).

ParB is functionally equivalent to kinetochore proteins in eukaryotic cells that are involved in chromosome segregation after replication, which also provide a link between the "centromere" (the *parS* sequence) and an NTPase (ParA in the ParABS system) (32). ParB has a DNA-binding domain (DBD) that contains a helix-turn-helix (HTH) motif that contains two helices that make contact with the major groove of a DNA double helix, and the second helix is called the recognition helix and contacts with specific base pairs in the binding sequence for a high level of binding specificity (17). Specific binding of ParB to *parS*-containing DNA has been shown to protect ParB fragments containing the HTH motif from proteolysis, whereas ParB bound to non-specific DNA sequences were not protected from proteolysis, indicating that there are different sites on the protein capable of binding DNA at different specificities (32, 39). Despite the high binding affinity displayed by ParB for parS sites, ParB does not associate with *parS* permanently, as indicated by its spreading ability (28, 31); rather, ParB likely disengages from the targeted *parS* site after binding to make space for another ParB molecule to engage with the now-free *parS* site (13, 41). The transient nature of the ParBS complex is further indicated by the steric clashing of a DNA molecule bound to one HTH motif with the other HTH motif in a ParB dimer is at odds with the high-specificity ParB-*parS* interaction, implying that once ParB has engages its NTDs around *parS*, the DNA disengages from the HTH motif (36).

DNA compaction is mediated by ParB and appears to involve the N-terminal domain (NTD) region of the protein, which contains a highly conserved GxxRxxA motif, with glycine being the 77th amino acid and arginine the 80th in *Bacillus subtilis* (2, 15, 43). The G77S and R80A mutations are in the highly conserved arginine-rich patch of the N-terminal ParB Box II (11, 44) and prevent the formation of compact foci in vivo while also losing the ability to spread along the DNA (15). The R80A mutant also was seen to abolish the DNA compaction ability in

vitro, and it also appeared to lack the ability to bridge DNA in vitro, but still retained the ability to bind to DNA (37). The arginine-rich patch in ParB has been implicated to be necessary for DNA bridging and nearest-neighbor interactions that facilitate ParB spreading on DNA (15, 37, 39). The ParB-compacted state of DNA is not a highly ordered complex and is not dependent on the presence of a *parS* sequence, implying that compaction requires the non-specific DNA binding activity of ParB (13). The R149G mutant in the HTH motif is unable to fully compact DNA by preventing ParB from specifically interacting with *parS* DNA, but surprisingly still retains the ability to bind non-specifically to and compact DNA without a *parS* site, indicating that there may be a second non-specific DNA binding locus in ParB (13).

A potential candidate for the non-specific binding activity of ParB in *Bacillus subtilis* is the C-terminal domain (CTD) binding locus (35). The CTD contains a lysine-rich surface that participates in non-specific DNA binding and is involved in DNA condensation in vitro and may also self-associate and allow ParB to dimerize via the CTD and play a role in both bridging interactions as well as DNA compaction (13, 37). Three lysine patches in the CTD were mutated in the full-length ParB protein (K252-K255-K259) to contain alanine residues, which abolished DNA compaction completely and caused the protein to fail to form ParB foci in vivo due to the inability to bind non-specific DNA while still localizing to the nucleoid region – potentially from the *parS*-specific HTH motif in the DBD remaining functional – unlike other mutants that prevent foci formation (13). The CTD has also been shown to disrupt ParBS partition complex formation and even induce decondensation (13, 27). A CTD "capping" model has been introduced where introducing free CTD proteins to bind to the CTD of a full-length ParB protein leave ParB able to bind to DNA but unable to compact it, likely due to the inhibition of proper ParB dimer formation required for ParBS complex formation (10, 27).

Along with its DNA-binding and condensing activity, ParB is also required to recruit ParA to a ParB-*parS* partition complex (11, 14, 21, 23, 29). ParA proteins use ATP binding to polymerize, and this binding may be stimulated by the NTD of ParB bound in a partitioning complex with *parS* DNA (3, 5, 9, 18, 30, 39, 42). ParA density is highest in the interior of the nucleoid region and is closely associated with the nucleoid locations of ParBS partition complexes, and ParA may play an instrumental role via its non-specific DNA binding ability and ATPase activity in localizing the partition complex in the bacterial nucleoid (21). Partition complexes (ParBS) for both plasmid and chromosomal DNA are located at the interior on the nucleoid region in the mid-cell area either during or after replication has occurred, and they segregate to new subcellular locations afterwards through the recruitment of ParA to non-specific DNA and stimulation of ParA ATPase activity by ParB in the condensed partition complex (14, 21, 28). ParA interacts with the partitioning complex via the NTD of ParB to stimulate ATP hydrolysis (32) to aid in faithful ATP-dependent DNA segregation and transportation of partitioning complexes after replication and during cellular division (33, 40).

The novel CTPase activity of BsParB modulates protein activity

Recently, paradigm shifting research showed that ParB is a novel CTP hydrolyzing protein, or CTPase, that uses the energy from CTP hydrolysis to likely modulate the DNA-binding activities of ParB in relation to *parS* sites (19, 36). The conserved GxxRxxA motif of the ATP binding pocket of an unrelated eukaryotic protein sulfiredoxin (Srx) is similar to the the NTD of ParB, with the crystal structure of NTD associating with a CDP molecule (likely hydrolyzed during the crystallization process). It is likely that a ParB dimer binds to at least two molecules of CTP (36). Superimposing the NTD of ParB with Srx shows a fair deal of overlap with where the phosphates in CDP interact with the NTD and where the ATP phosphates interact

with Srx (4, 20, 36). The Srx/ATP binding pocket also coordinates with a Mg^{2+} ion, which implies that it is likely that a Mg^{2+} ion likely will have a stabilizing effect on the triphosphate moiety of CTP (29, 36). The β-phosphate of CTP makes contact with the R80 residue (36). The R80A mutant – aside from being a spreading- and DNA bridging-deficient mutant than cannot compact DNA or form foci in vivo – was also shown to be a CTP binding mutant than cannot bind CTP (15, 36, 37, 39).

ParB in *B. subtilis* is able to hydrolyze roughly five molecules of CTP every hour, and when *parS* DNA was introduced the hydrolysis rate increased to about 36 CTP molecules per hour (36). The CTP hydrolysis rate of Caulobacter increased from an average of 0.4 molecules of CTP hydrolyzed to 3 CTP hydrolyzed per hour when *parS* DNA was introduced (19). These data provide exciting evidence that *parS* DNA stimulates the CTPase activity of ParB. To test the effect of CTP binding/hydrolysis on NTD dimerization, ParB dimers were cross-linked at T22C with bismaleimidoethane (BMOE), and strong cross-linking of the NTDs was only observed with the presence of both CTP and *parS* sites on the DNA to produce mostly ring-shaped ParB dimers. This implies that the NTD of ParB is a CTP-dependent gate that closes specifically around *parS* DNA, with *parS* DNA acting as the catalyst for the CTP-dependent closure (36). These findings are incorporated into a model for ParB-mediated DNA condensation that shows the NTDs of two ParB proteins interacting to "cage" the *parS* site while the CTDs of those ParB proteins interact with other CTDs to entrap non-specific DNA (37).

The CTP binding pocket on ParB also plays a role in assisting in ParA recruitment (39). The Myxococcus xanthus species has a protein called PadC which contains a ParB/Srx-like (MxParB) domain – which is analogous to the NTD – that has a lot of similarities to the ParABS system (25). Mutations of arginine residues in the CTP binding pocket on this PadC protien

showed aberrant ParA localization patterns, and in many cases showed a complete reduction of ParA recruitment when multiple arginine residues were mutated, which implies that PadC's MxParB/Srx domain is stabilized by CTP in order to enable proper interaction between PadC and ParA (29). The non-hydrolyzable CTPγS increased the stability of the ParB/SRX domain, as well as the HTH motif in the DBD of MxParB, which suggests that CTP binding is important for specific DNA-binding and binding affinity (29).

ParB's spreading ability is also modulated by its CTPase activity with the evidence that CTP binding assists in ParB disengaging from *parS* DNA (19). The CTP hydrolysis activity of ParB seems to circumvent this obstacle by helping ParB unload from DNA that is "off-target" from the *parS* site (1, 19). Also, ParB does have the ability to engage its NTDs in a *parS*-independent manner with CTP binding (36). The idea that ParB can form an NTD-dimerized gated ring that closes indiscriminately can be troublesome if ParB dimers were to close before they were able to load onto DNA, which would effectively remove them from the pool of available protein (1). CTP hydrolysis can also avoid a high proportion of DNA-free ring dimers that are unable to participate in chromosomal compaction and segregation (1)

Single-molecule methods and TIRF microscopy

Total internal reflection fluorescence (TIRF) microscopy is a useful imaging tool that can image fluorescent molecules with a high degree of selectivity. Using Snell's Law $n_1 \sin\theta_1 = n_2 \sin\theta_2$ to calculate the critical angle $\theta_{critical} = \sin^{-1}(n_1/n_2)$ will generate the angle at which the light from the laser beam will be totally reflected when incident from a material with higher index of refraction n_2 to that with lower index of refraction n_1. This total reflection generates an evanescent field with a rapid exponential decay that will illuminate the sample so that the only fluorescent molecule that are excited are ones 100-200 nm above the coverglass-water interface

(12). This manner of illuminating biological samples is ideal for single molecule experiments where fluorescently labeled single molecules (proteins or nucleic acids near the flowcell surface are being examined in a flowcell apparatus.

CHAPTER III

METHODOLOGY AND FINDINGS

Protein Purification

Purification of ParB(WT) and ParB(R80A)

Proteins were provided by HyeongJun Kim according to protocols established by Graham et al. (15) and Song et al. (37) for both the wildtype ParB(WT) and recombinant mutant ParB(R80A). Importantly, proteins were treated with apyrase during the purification process to deplete any nucleoside triphosphates that may otherwise be co-purified.

H6-SUMO-KCK tagging of WT and R80A (N-terminus, C-terminus)

The addition of a lysine-cysteine-lysine (KCK) tag to the N-terminus of the wildtype ParB protein (ParB(KCK-WT)) allows for additional fluorescent molecule tagging, such as with a cysteine-containing maleimide-Cy3 dye. The *Bacillus subtilis* ParB contains no cysteine in its amino acid sequence, making the KCK tag a specific location for maleimide-Cy3 labeling vis disulfide bridge formation. For in vivo experiments, the addition of a KCK tag to the N-terminus of ParB was shown to not affect DNA binding or foci formation (15). Another version of ParB with the C-terminus tagged with a KCK tag (ParB(WT-KCK)) was also purified. The recombinant ParB(R80A) protein was also tagged with a KCK tag on either the N-terminus or C-terminus.

Cy3 tagging of WT and R80A to ~50% labeling efficiency

To see fluorescently tagged proteins that do not have a terminally appended KCK tag, we labeled the proteins non-specifically with a NHS-ester version of the Cy3 dye rather than the Cy3-maleimide dye. In physiological conditions, this version of Cy3 has been known to be biased toward binding on the N-terminus.

Single-Molecule Flow-Stretching Experiments

PEGylation of microscope slides

Flowcell construction begins with PEGylation of coverslips. Coverslips are cleaned gently with air before being placed in a polypropylene coplin staining jar with five subspaces, with one coverslip per subspace. Typically, four jars with a total of 20 coverslips are prepared at a given time. The jar is filled with 200 proof ethanol and sonicated for 30 minutes. After sonication, the ethanol is disposed of, and the coverslips and jar are rinsed with MilliQ water for a minimum of five times. The jar is then filled with 0.5 M potassium hydroxide (KOH) and sonicated for 30 minutes, after which the KOH is disposed of, and the jar and coverslips are rinsed with MilliQ water for a minimum of 5 times. The coverslips that are in contact with the walls of the jar are rotated to ensure that both sides of the coverslip are adequately cleaned. Both the ethanol and KOH wash are repeated, resulting in a total of four sonication cycles. The cleaned coverslips are stored in MilliQ water.

After cleaning, the coverslips are silanized with (3-Aminopropyl)triethoxysilane and pegylated mPEG/biotin-PEG. Before silanization, (3-Aminopropyl)triethoxysilane is removed from its 4 °C storage and mPEG/biotin-PEG from its -20 °C storage and allowed to reach room temperature to prevent condensation from reacting with the chemicals. A laboratory oven clean

oven racks inside is heated to 110 °C. The coverslips must have all traces of water removed before silanization, so the water is discarded and the jars are filled with acetone. The lids of the jars are rinsed separately with acetone. After the first wash, the acetone wash is repeated twice more. During the third and last acetone wash, the jars and coverslips are sonicated for 10 minutes.

A ~2% (v/v) silane solution is prepared by mixing 4.4 mL of (3-Aminopropyl)triethoxysilane with 220 mL acetone for the four jars of coverslips being made. The (3-Aminopropyl)triethoxysilane vial is immediately placed into a vacuum pump and filled with argon gas before being stored again at 4 °C. The solution is immediately poured into the jar and the jar closed, and the jars are shaken while being turned 90° every 20 seconds for a total of 2 minutes to ensure that the coverslips are completely silanized. The solution is disposed of in the appropriate waste container and the silanization reaction is immediately quenched with a minimum of 1-2 liters of MilliQ water per jar.

Each silanized coverslip is then placed in the heated oven on the racks to dry for 30 minutes. When the coverslips are dry, they are labeled with a lowercase “a” on two corners and an uppercase “F” on the other two corners to help identify with sides are coated with PEG, with the non-coated side having the proper-facing letters written on it and the PEG-coated side on the opposite side of the coverslip.

While the coverslips are drying, 25 mL of 100 mM sodium bicarbonate ($NaHCO_3$) is prepared and placed on ice. A tube with 6.8 mg of biotinylated PEG and 170 mg of mPEG for the 20 coverslips is prepared and placed in -20 °C until needed later. Once the coverslips are dry, 1100 μL of 100 mM $NaHCO_3$ are added to the tube containing the mPEG/biotin-PEG mixture and placed on ice, and 100 μL of the PEG-$NaHCO_3$ solution is pipetted onto a silanized

coverslip. A second coverslip is placed gently on the first coverslip to sandwich the PEG-$NaHCO_3$ solution between them. This is repeated for all 20 coverslips. The coverslips are placed in repurposed pipette tip boxes with MilliQ water in the bottom of the box to prevent the coverslips from drying out. The PEGylation occurs for 2 hours in a dark place. Meanwhile, another tube of mPEG/biotin-PEG is prepared for a second round of PEGylation and left at -20 °C. After 2 hours, 1100 μL of sodium bicarbonate is added to the PEG mixture, the sandwiched coverslips are gently separated and an additional 100 μL of the PEG solution is added. The sandwiched coverslips are returned to their box and left for an addition 2 hours for a total time of 4 hours.

The sandwiched PEGylated coverslips are gently separated and rinsed with a gentle stream of MilliQ water from a handheld squeeze-bottle, and then gently dried with compressed air. Once thoroughly dried, the PEGylated coverslips are stored at -80 °C until they are needed for flowcell construction.

Flowcell construction

A quartz-top microscope slide is prepared by drilling four holes corresponding to a two-channel template. Using the same template, two rectangles are cut from double-sided tape in order to make the two flowcell channels, and the tape is placed on the quartz-top slide. Any bubbles are scraped out using a blunt and flat instrument. Inlet tubing that is 7 cm long and outlet tubing that is 2.5 cm long are prepared for each channel, with each tube having one end cut at a 30° angle.

A PEG-coated coverslip is removed from the freezer and cut in half widthwise, with one half being used per flowcell. If the coverslip appears to have spots of dried condensation, it can

be gently rinsed with MilliQ water and dried with compressed air. The quartz-top slide is then sandwiched to the PEG-coated coverslip, taking care to ensure than the side with the PEG coating is placed directly on the tape to make the channel. Any bubbles are gently removed, taking care to not crack the delicate PEG-coated coverslip. One inlet tube and one outlet tube are inserted into the flowcell channel with their cut ends facing each other . 5-minute epoxy is used to carefully seal the edges of the flowcell and fix the inlet and outlet tubing in place, taking care to leave the bottom of the flowcell level.

Quantum dot labeled DNA experiments

Single-molecule flow-stretching experiments are conducted on a total internal reflective fluorescence (TIRF) microscope with an electron multiplying CCD camera and a 532 nm laser. Exposure time for recorded movies is 100 milliseconds but taken every 200 milliseconds, or 5 frames per second. The 100x 1.49 NA objective without additional magnification was used with immersion oil type-F. EM gain of the camera is set to 1000, and the laser power is set to 10%, which is 10 mW. The chamber of the flowcell is placed on the microscope objective, with the chamber running horizontally across the objective.

Bacteriophage lambda DNA that is 46.5 kpb long, both with and without *parS* sites, that have 12-nucleotide overhangs on both ends of the DNA are used. Biotin is annealed and ligated to one end of the DNA and digoxigenin is annealed and ligated to the other end to make BL1-Dig2-Lambda-DNA or BL1-Dig2-*parS*-DNA. Buffers used are EcoRI Binding Buffer (EBB buffer, 10 mM Tris, pH 8.0, 150 mM NaCl, 10 mM MgCl2) supplemented with 0.2 mg/mL Bovine Serum Albumin (EBB+BSA), and ParB100 Buffer (10 mM Tris, pH 7.5, 100 mM NaCl, and 2.5 mM MgCl2), and all are held on ice. Buffers are placed in a vacuum pump on ice for a

minimum of 1 hour before experiments in order to remove any bubbles from the buffers. CTP and CTPγS stocks are stored in -80 ˚C.

For experiments, 0.7 μL of BL1-Dig2-Lambda-DNA or BL1-Dig2-*parS*-DNA is incubated with 0.3 μL of anti-digoxigenin antibody-conjugated Quantum dot 605 (Qdot) in the presence of 19 μL of EBB+BSA buffer for 5 minutes on ice, making 20 μL total volume in a 1.5 mL tube. When pipetting the DNA, about 2 mm on a 200 μL pipette tip is cut off to make the hole wider for the purpose of preventing any shear damage to the length of the DNA. While the DNA and Qdots incubate, prepare 120 μL of a 0.25 mg/mL neutravidin solution (30 μL of 1 mg/mL neutravidin and 90 μL EBB+BSA buffer). Next, 58 μL of neutravidin+EBB+BSA are pipetted into each flowcell chamber and incubated for 5 minutes at room temperature to react with the biotin on the PEG-coated coverslip which will provide binding sites for the biotin end (BL1) of the DNA. The inlet and outlet tubing are sealed with needles that have been sealed with epoxy.

After the flowcell has been incubated with neutravidin, a needle from an outlet tube is removed and replaced with tubing attached to a syringe pump via an air spring. The needle from the inlet tubing is then removed, and the tubing is placed into a 1.5 mL tube containing EBB+BSA buffer. The flowcell is washed by manually pulling the syringe and rapidly flowing 200-300 μL of EBB+BSA buffer through to remove excess neutravidin and any bubbles trapped in the flowcell. An additional amount of 100 μL EBB+BSA can be flowed through the flowcell at 300 μL/min to ensure there are no bubbles in the flowcell.

A 200 μL pipette tip that with the tip cut is used to transfer 10 μL of the DNA mixture to a separate 1.5 mL tube and set aside on ice for a subsequent experiment. 500 μL of EBB+BSA buffer is added to the 10 μL of the DNA solution, which replaces the 1.5 mL tube containing

EBB+BSA buffer. The transfer of tubes must be done quickly and with minimal movement to ensure that no air bubbles are introduced into the inlet tubing. The solution of DNA is then flowed through the flowcell at a rate of 30 μL/min until a good number of DNAs are tethered to the PEG-coated coverslip. Flow can be periodically stopped for 2-3 minutes at a time to allow for binding to occur, using the 532 nm laser to visualize the Qdots. After a good number of DNAs are tethered, a 1.5 mL tube containing ParB100 buffer replaces the solution DNA, and 200 μL of ParB100 buffer is flowed through at a rate of 50 μL/min to remove excess unbound DNAs and Qdots. If a large number of Qdots are non-specifically bound to the PEG slide, laser power can be increased briefly in an attempt to remove them from the PEG slide.

Once the flow is clear of excess DNAs and Qdots, the control movie is recorded. The frames to be recorded are set to 300, but there is no flow for the first 100 frames. Flow is only started after 100 frames have been recorded to show the behavior of the DNA when there is no flow and then how the DNA looks when flow is introduced to stretch them. After the control movie has been recorded, a solution of the protein being tested is prepared in ParB100 buffer to correspond to the molarity being tested (50 nM, 30 nM, etc.). For example, to make a 200 μL of a 50 nM solution from 9.58 μM ParB(WT) stock, 1.04 μL of 9.58 μM WT BsParB will be added to 198.96 μL ParB100 buffer. If the experiment contains 1 mM CTP, the ratios would be 1.04 μL of 9.58 μM WT BsParB with 2.00 μL of 100 mM CTP in 196.96 μL ParB100 buffer. When adding the protein and 100 mM CTP to the bottom of a 1.5 mL tube, care must be taken to not let them touch before the ParB100 buffer is added. Once ParB100 buffer is added, the ParB solution or ParB and CTP solution is allowed to incubate on ice for 1 minute before flowing the solution through the flowcell.

While the solution is incubating, the frames for the experiment are set to a large number and the syringe pump is set to the withdraw the exact volume of the experiment (for example, 1200 frames for an experiment volume of 200 μL flowed at 50 μL/min). The tube with ParB100 buffer is replaced by the experiment tube. Once flow is started, the movie is recorded for the duration of the experiment. If the experiment is over before the movie is set to finish, the movie can be stopped, but flow through the syringe pump must continue. This is another control step, where the confirmation that the entire volume of the experiment was flowed through indicates that there was no occlusion caused by bubbles or defects in the flowcell.

Both the control and experiment movies are saved as a TIFF file with a descriptive name inside of a folder with the same name. For example, an experiment of wild type BsParB at 50 nM concentration on lambda DNA without CTP conducted on 01/03/2022 in chamber 1 of the flowcell would have movies named “20220103(1)-ParB(WT)-50nM-lambda_DNA-CTP0mM-control” and “20220103(1)-ParB(WT)-50nM-lambda_DNA-CTP0mM-experiment”. Excess frames are cropped if necessary to shorten the movie to the exact number of frames of the experiment. The flowcell is removed from the microscope objective and the objective is cleaned with methanol and lens cleaning paper. The syringe pump tubing is removed from the outlet tubing of the flowcell and placed into a 50 mL falcon tube containing MilliQ water, which is then flushed at a rate of 3000 μL/min with 1500 μL of MilliQ water. The syringe pump tubing is disconnected from the syringe and all contents of the syringe are manually ejected into a waste container. Now the microscope is ready for another experiment in the second chamber of the flowcell.

Cy3-labeled protein experiments

Single-molecule flow-stretching experiments are conducted on a total internal reflective fluorescence (TIRF) microscope with an electron multiplying CCD camera and a 532 nm laser. Exposure time for recorded movies is 100 milliseconds but taken every 200 milliseconds, or 5 frames per second. The 100x 1.49 NA objective without additional magnification was used with immersion oil type-F. EM gain of the camera is set to 1000, and the laser power is set to its lowest power of 1%. A neutral density filter of 0.5 is used to further lower the power of the laser.

The Cy3-labeled protein experiments are similar to the Qdot-labeled DNA experiments. Bacteriophage lambda DNA, both with and without *parS* sites, that have 12-nucleotide overhangs on only one end of the DNA are used. Biotin is annealed to the end of the DNA to make BL1-Lambda-DNA or BL1-*parS*-DNA. Buffers used are EcoRI Binding Buffer supplemented with 0.2 mg/mL Bovine Serum Albumin (EBB+BSA), ParB100 Buffer containing 0.02 mg/mL of BSA (ParB100+BSA), and ParB100 buffer containing 0.2 mg/mL BSA and a 0.05X dilution casein prepared from a 10X casein solution (ParB100+BSA+casein), and all are held on ice. Adding BSA and casein to the ParB100 imaging buffer prevents the Cy3-labeled protein from sticking to the PEG-coated coverslip. Buffers are placed in a vacuum pump on ice for a minimum of 1 hour before experiments in order to remove any bubbles from the buffers.

For experiments, 0.7 μL of BL1-Lambda-DNA or BL1-*parS*-DNA is added to 244.3 μL of EBB+BSA buffer for 5 minutes on ice, making 250 μL total volume in a 1.5 mL tube. When pipetting the DNA, 2 mm of a 200 μL pipette tip is cut off to make the hole wider for the purpose of preventing any shear damage to the length of the DNA. 120 μL of a 0.25 mg/mL neutravidin solution is prepared. Next, 58 μL of neutravidin+EBB+BSA are pipetted into each flowcell chamber and incubated for 5 minutes at room temperature.

After the flowcell has been incubated with neutravidin, a needle from an outlet tube is removed and replaced with tubing attached to a syringe pump via an air spring. The needle from the inlet tubing is then removed, and the tubing is placed into a 1.5 mL tube containing EBB+BSA buffer. The flowcell is washed by manually pulling the syringe and rapidly flowing 200-300 μL of EBB+BSA buffer through to remove excess neutravidin and any bubbles trapped in the flowcell. An additional amount of 100 μL EBB+BSA can be flowed through the flowcell at 300 μL/min to ensure there are no bubbles in the flowcell.

After excess neutravidin has been washed away, 200 μL of the solution of DNA in EBB+BSA is then flowed through the flowcell at a rate of 30 μL/min, after which flow is stopped for 4 minutes to allow DNA to bind to the PEG-coated slide. Since there are no fluorescent molecules on the DNA, the 532 nm laser cannot be used to visualize DNA binding. After 4 minutes have passed, 140 μL of ParB100+BSA+casein buffer is flowed through at a rate of 50 μL/min to remove excess unbound DNA. After, 140 μL of ParB100+BSA without casein is flowed through to wash away excess casein.

There is no control movie recorded for the Cy3-labeled protein experiments, so the experiment is set up directly. A solution of the protein being tested is prepared in ParB100 buffer to correspond to the molarity and conditions being tested. Once ParB100+BSA buffer is added, the ParB solution or ParB and CTP solution is allowed to incubate on ice for 1 minute before flowing the solution through the flowcell.

The frames for the experiment are set to a large number and the syringe pump is set to the withdraw the exact volume of the experiment. The tube with ParB100 buffer is replaced by the experiment tube. Care must be taken to focus the microscope carefully before the experiment begins. Once flow is started, the movie is recorded for the duration of the experiment. If the

experiment is over before the movie is set to finish, the movie can be stopped, but flow through the syringe pump must continue.

Once the movie is saved as a TIFF file with a descriptive name, excess frames are cropped if necessary to shorten the movie to the exact number of frames of the experiment. The flowcell is removed from the microscope objective and the objective is cleaned with methanol and lens cleaning paper. The syringe pump tubing is removed from the outlet tubing of the flowcell and placed into a 50 mL falcon tube containing MilliQ water, which is then flushed at a rate of 3000 μL/min with 3000 μL of MilliQ water. The syringe pump tubing is disconnected from the syringe and all contents of the syringe are manually ejected into a waste container. Now the microscope is ready for another experiment in the second chamber of the flowcell.

Compaction Analysis

Using ImageJ (FIJI) to select Qdot Regions of Interest

Movies saved as a TIFF file are analyzed by ImageJ software to select regions of interest (ROIs) that contain compacting DNA for later analysis. The folder where the movie is saved is prepared with the following folders inside: "2 > Analysis > QD". If the DNA compaction is not as vertical as possible with the compaction trajectory in the Y direction, the movie can be rotated using ImageJ. The "Image" tab is selected, then "Transform > Rotate…" are selected to rotate the movie. A new movie is saved as a TIF file with the number of degrees rotated included in the file name, which is saved in the same folder as the original movie.

To properly select ROIs for measurement, the "Analyze" tab is selected on the software to set the measurement to "Area" and "Bounding Rectangle". After an ROI is selected using the smallest rectangle possible that contains the entire path of a Quantum dot that shows a DNA

compaction event, “Ctrl+t” is pressed to place the ROI coordinates in the ROI manager. This step is repeated until every analyzable DNA ROI is selected. DNAs that appear to stop compacting prematurely by becoming stuck to the PEG slide or by interacting with neighboring DNAs, or DNAs that become untethered during the course of the experiment, are not selected for analysis. In the ROI manager, every ROI coordinate is selected and measured to give the area, width, height, and X and Y-coordinates of each DNA ROI. The results are saved as a text file with a descriptive title containing the date of the experiment, for example “20220103(1)QDRoi.txt”. Importantly, do no close the ROI manager yet.

Next, background ROIs that correspond to each DNA ROI are selected in the same manner, using the smallest possible square as close to the DNA ROI that does not have any signal from a Quantum dot. After each background ROI is selected, each one is selected in the ROI manager and measured. The results are saved as “20220103(1)BGRoi.txt”. Both text files will be used with MATLAB for analysis. Now all ROIs in the ROI manager are selected and saved as a zip file by clicking “More > Save…” on the ROI manager and named “20220103(1)RoiSet.zip”. This zip file can be dragged onto ImageJ to overlay each ROI on the movie file.

With the movie file still open, the file is saved by clicking “File > Save As > Image Sequence…” in folder “2” to save each frame of the movie as a TIF file for analysis. The number in the “Start At” box is changed from “0” to “1” and the file name must end with a dash, so that each TIF image saved ends with a four-digit number that corresponds to its frame number; for example, “20220103(1)-ParB(WT)-50nM-lambda_DNA-CTP0mM-experiment-0001” for the first frame in the movie. Next, an average composite image of the movie is generated by clicking “Image > Stacks > Z Project > Average Intensity” and is saved in the same folder with a name

beginning with “AVG_” to give a file name like “AVG_20220103(1)-ParB(WT)-50nM-lambda_DNA-CTP0mM”. Now the compaction rate is ready to be analyzed via MATLAB.

Using MATLAB to track and calculate compaction rate

MATLAB codes were provided by HyeongJun Kim. The code “qdot_track.m” is used to track the signal intensity of the fluorescent quantum dot against the lack of signal from the background of the movie. The code allows for every ROI to be analyzed, but individual ROIs can also be selected and cropped if there is a non-specifically bound Qdot in the ROI that would interfere with the tracking. Running the code prompts the user to select the directory that has the images to be analyzed. The starting frame is set as “1”, the ending frame is set to the last frame of the movie being analyzed, the frame increment is set as “1” and the timer per frame in seconds is set at “0.2” frames per second. Next, the Qdot text file and the Background text file are selected. Next, the background multiplication factor, or threshold for Qdot signal analysis against the background signal, is set at “2.6” for most analyses. The multiplication factor can be increased if the signal intensity of a particular movie is low. Next, a directory location is selected to save the output of the tracking code and the desired output name is fed into the code. Now the code is ready to be run and generate Qdot time vs. trajectory files.

Once the time vs. trajectory files for each ROI are acquired, the next code “artifact_removal_4chanced.m” is used to remove any artifact signal intensity that is not from the Qdot trajectory. An example of a time vs. trajectory file is shown in. If the artifact data points are too numerous, the file can be cropped and analyzed individually with the “qdot_track.m” code previously described. A folder with the time vs. trajectory text files is selected and then the new converted time vs. trajectory files are saved to a new folder, such as “Analysis”. The code generates an average trajectory path overlayed on the new time vs. trajectory files.

The code “hjkim_fit_Qdot_20210110.m” will analyze the averaged trajectories generated previously. Two points on the slope of the curve that are associated with the beginning of compaction and the end of compaction are selected to generate the compaction rate. This is repeated for every averaged trajectory file, after which an Excel file is generated that contains the calculated compaction rate for each ROI in the movie. Data from the Excel file can be analyzed using Microsoft Excel or GraphPad Prism 9 software.

Using GraphPad Prism 9 for graphing and statistics

GraphPad Prism software was used to do statistical analysis on compaction rates generated by MATLAB analysis, as well as generating graphs for visual comparison purposes. All error bars represent the standard error of the mean (SEM). Statistics used for analysis include descriptive statistics shown in Table 1 and Table 2, as well as t-tests shown in Table 3 and Table 4 for determining statistical significance between mean compaction rates. All statistical tables are in Appendix A.

Findings

ParB(WT) Quantum dot experiments

Three different wild type BsParB proteins were tested: a version with a lysine-cysteine-lysine (KCK) tag terminally appended to the N-terminal domain (ParB(KCK-WT)), a version with a KCK tag terminally appended to the C-terminal domain (ParB(WT-KCK)), and an untagged version (ParB(WT)). All three proteins were tested on BL1-Dig2-Lambda-DNA with no *parS* site or on BL1-Dig2-*parS*-DNA containing one *parS* site in the middle of the DNA, with ParB100 buffer conditions containing either no CTP, 1 mM CTP, or 1 mM CTPγS. The untagged ParB(WT) protein was tested at various concentrations of 50 nM, 30 nM, and 10 nM to see the effect of protein concentration on DNA compaction rate, while both tagged ParB(KCK-WT) and ParB(WT-KCK) proteins were tested at the 50 nM concentration only. Averaged compaction rates for all conditions tested are showed in Table 1 in Appendix A, which are graphed below in Figure 1. Additional figures are located in Appendix A.

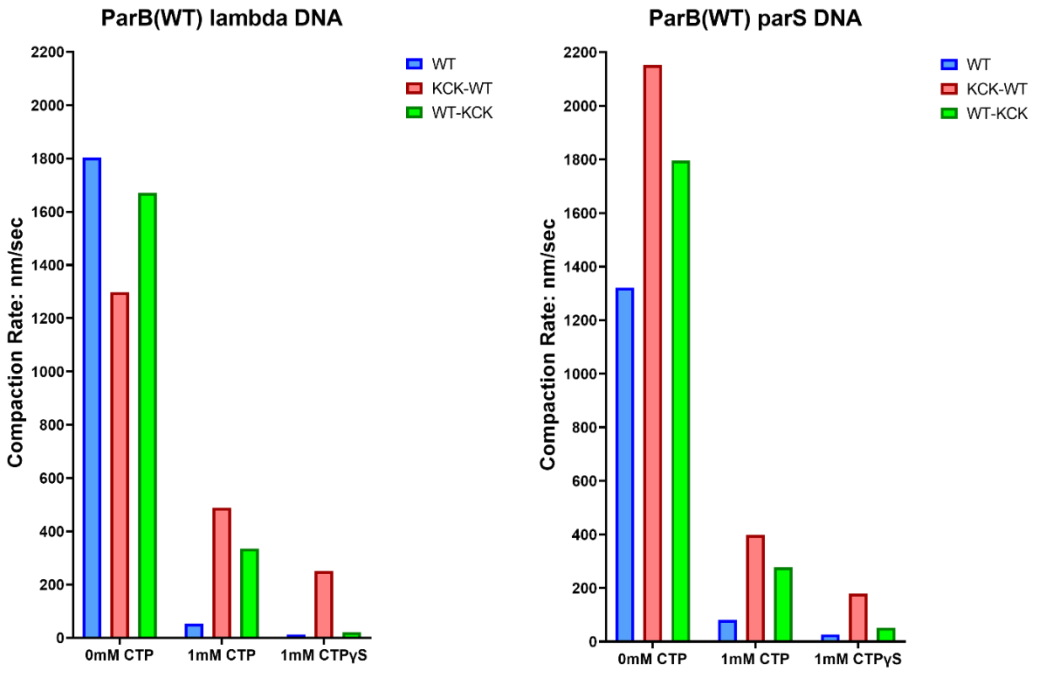

Figure 1. Overall results of tagged and untagged ParB(WT) on bacteriophage lambda DNA and lambda DNA containing a single *parS* site, in the presence of 0 mM CTP, 1 mM CTP, and 1 mM CTPγS.

The DNA compaction rates by both tagged and untagged ParB(WT) for lambda DNA and *parS* DNA were measured and compared in the absence of CTP. On lambda DNA, both the KCK-WT and WT-KCK show slowed down compaction rates compared to the untagged WT, while the WT-KCK is faster than the KCK-WT. On *parS* DNA, both the KCK-WT and WT-KCK speed up when compared to the WT, while the WT-KCK is slower than the KCK-WT. This pattern shows that a KCK tag produces artifact compaction rates when compared to the untagged WT with no CTP present. The untagged WT slows down on *parS* DNA when compared to the WT on lambda DNA, while both the KCK-WT and WT-KCK speed up on *parS* DNA compared to their lambda DNA counterparts (Figures 4, 10-12).

In the presence of 1 mM CTP on lambda DNA, each protein tested had a slower compaction rate than protein in the absence of CTP. The addition of a *parS* site to the DNA did not change this pattern. On lambda DNA, both the KCK-WT and WT-KCK speed up when compared to the WT, but the WT-KCK is slower than the KCK-WT. On *parS* DNA, both the KCK-WT and WT-KCK speed up when compared to the WT, but the WT-KCK is slower than the KCK-WT. This is a pattern that shows that the addition of a KCK tag produces artifact compaction rates when compared to the untagged WT with 1 mM CTP present. The WT on *parS* DNA is slightly faster than the WT on lambda DNA, whereas both KCK-WT and WT-KCK are slower on *parS* DNA than their counterparts on lambda DNA are (Figures 5, 10-12).

All proteins tested on both lambda DNA and *parS* DNA have a slower DNA compaction rate in the presence of 1 mM CTPγS than they do in the 0 mM CTP and 1 mM CTP conditions. On lambda DNA, both the KCK-WT and WT-KCK speed up compared to the WT, while the KCK-WT is much faster than the WT-KCK; the WT-KCK is only marginally faster than the WT. On *parS* DNA, both the KCK-WT and WT-KCK also speed up when compared to the WT, while the WT-KCK is much slower than the KCK-WT; again, the WT-KCK is not much faster than the WT. This pattern shows that a KCK tag produces artifact compaction rates when compared to the untagged WT with 1 mM CTPγS present. The untagged WT speeds up on *parS* DNA when compared to the WT on lambda DNA, the KCK-WT slows down on *parS* DNA when compared to KCK-WT on lambda DNA, and WT-KCK speed up on *parS* DNA compared to its lambda DNA counterpart (Figures 6, 10-12).

When testing the effect of protein concentration on DNA compaction rates by untagged ParB(WT), the general pattern observed showed that decreasing the concentration of the untagged ParB(WT) resulted in a decrease in the compaction rate. The condition testing 1 mM

CTPγS on *parS* DNA shows an exception where the 30 nM condition was faster than the 50 nM condition, but a paired t-test result showed that these results were not significantly different (Figure 9). When comparing the compaction rates of the 50 nM and 30 nM ParB(WT) conditions between DNA types, the consistent pattern is that DNA compaction by ParB(WT) is slower on *parS* DNA than on lambda DNA when there is no CTP present, while showing faster compaction in the presence of 1 mM CTP and in the presence of 1 mM CTPγS. The 10 nM ParB(WT) condition consistently showed a faster compaction rate on *parS* DNA than on lambda DNA for a CTP conditions tested (Figures 7-9).

ParB(R80A) Quantum dot experiments

Three different R80A mutant BsParB proteins were tested: a version with a lysine-cysteine-lysine (KCK) tag terminally appended to the N-terminal domain (ParB(KCK-R80A)), a version with a KCK tag terminally appended to the C-terminal domain (ParB(R80A-KCK), and an untagged version (ParB(R80A)). All three proteins were tested on BL1-Dig2-Lambda-DNA without *parS* sites or on BL1-Dig2-*parS*-DNA containing one *parS* site, with ParB100 buffer experimental conditions containing either no CTP or 1 mM CTP. The untagged ParB(R80A) protein and both tagged ParB(KCK-R80A) and ParB(R80A-KCK) proteins were tested at the 50 nM concentration only. An additional experimental ParB100 buffer condition where Mg^{2+} ions were removed from the ParB100 buffer (ParB100WM buffer where WM stands for "without magnesium ions") was tested on the untagged ParB(R80A). Averaged compaction rates for all conditions tested are showed in Table 2 and graphed on Figure 2. Additional figures are located in Appendix A.

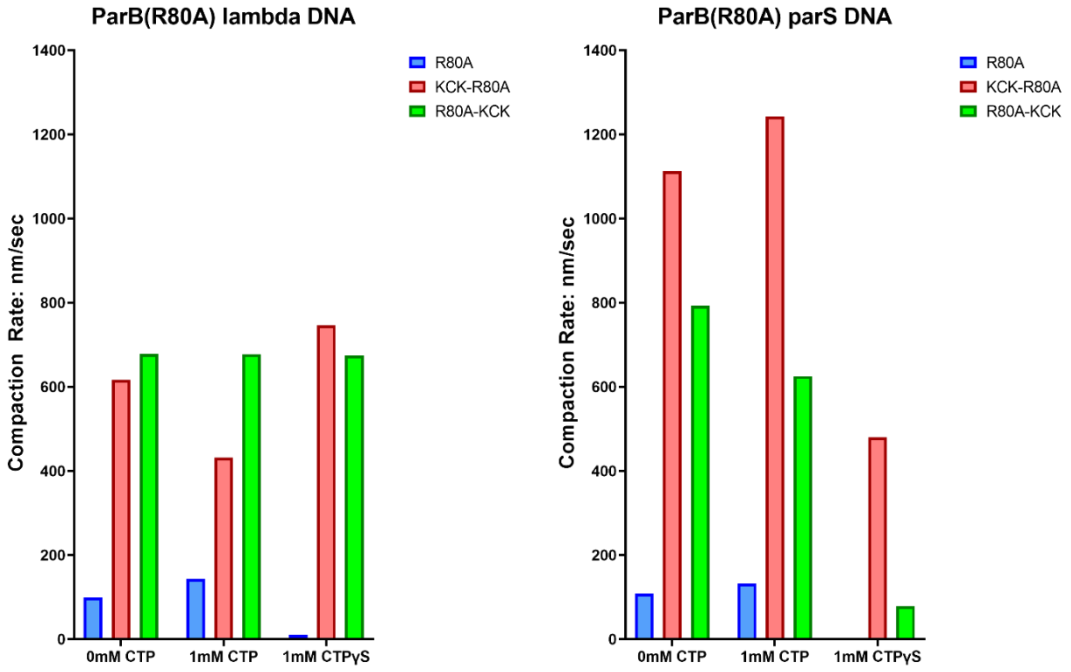

Figure 2. Overall results of tagged and untagged ParB(WT) on bacteriophage lambda DNA and lambda DNA containing a single *parS* site, in the presence of 0 mM CTP, 1 mM CTP, and 1 mM CTPγS.

The effect of 0 mM CTP on the ability of both tagged and untagged ParB(R80A) to compact lambda DNA and *parS* DNA was compared. On lambda DNA, both the KCK-R80A and R80A-KCK speed up compared to the untagged R80A. On *parS* DNA, both the KCK-R80A and R80A-KCK speed up when compared to the untagged R80A, while the R80A-KCK is slower than the KCK-R80A. This pattern shows that a KCK tag produces artifact compaction rates when compared to the untagged R80A with no CTP present. The untagged R80A has roughly the same compaction rate on *parS* DNA when compared to the R80A on lambda DNA, while both the KCK-R80A and R80A-KCK speed up on *parS* DNA compared to their lambda DNA counterparts (Figures 13, 16-18).

In the presence of 1 mM CTP, both the KCK-R80A and R80A-KCK speed up when compared to the untagged R80A, and the R80A-KCK is faster than the KCK-R80A on lambda DNA. On *parS* DNA, both the KCK-R80A and R80A-KCK speed up when compared to the untagged R80A, but contrary to the results with lambda DNA, R80A-KCK is slower than the KCK-R80A. This is a pattern that shows that the addition of a KCK tag produces artifact compaction rates when compared to the untagged R80A with 1 mM CTP present, and actually follow a similar pattern as the 0 mM CTP condition. The compaction rate of the untagged R80A on *parS* DNA is roughly the same as the untagged R80A on lambda DNA, whereas the KCK-R80A is faster on *parS* DNA, and R80A-KCK are slower on *parS* DNA than their counterparts on lambda DNA are (Figures 14, 16-18).

On lambda DNA, both the KCK-R80A and R80A-KCK speed up dramatically compared to the near-zero compaction rate of the untagged R80A in the presence of 1 mM CTPγS. On *parS* DNA, both the KCK-R80A and R80A-KCK also speed up when compared to the near-zero compaction rates of the untagged R80A, while the R80A-KCK is much slower than the KCK-R80A. This pattern shows that a KCK tag produces artifact compaction rates when compared to the untagged R80A with 1 mM CTPγS present. The untagged R80A has comparable compaction rates on lambda and *parS* DNA and both are near zero. The KCK-R80A slows down on *parS* DNA when compared to KCK-R80A on lambda DNA, and R80A-KCK slows down dramatically on *parS* DNA when compared to its lambda DNA counterpart (Figures 15, 16-18).

Generally, the addition of a lysine-cysteine-lysine (KCK) tag to either the N-terminus or to the C-terminus of both the wildtype and the mutant R80A ParB protein has shown that the tag does alter the characteristics of the protein function.

The effect of removing Mg^{2+} ions from the ParB100 imaging buffer produced a pattern of compaction rates that are the same for the compaction of both lambda and *parS* DNAs. In the absence of CTP, removing Mg^{2+} ions from the buffer resulted in a 6.77-fold increase of the compaction rate on lambda DNA and a 7.02-fold increase on *parS* DNA. Removing Mg^{2+} ions in the presence of 1 mM CTP results in a 4.71-fold and 5.76-fold reduction of the compaction rate on lambda DNA and *parS* DNA, respectively. Removing Mg^{2+} ions from the buffer in the presence of 1 mM CTPγS does increase the compaction rate, but the effect is more pronounced on *parS* DNA than on lambda DNA (Figures 19-21).

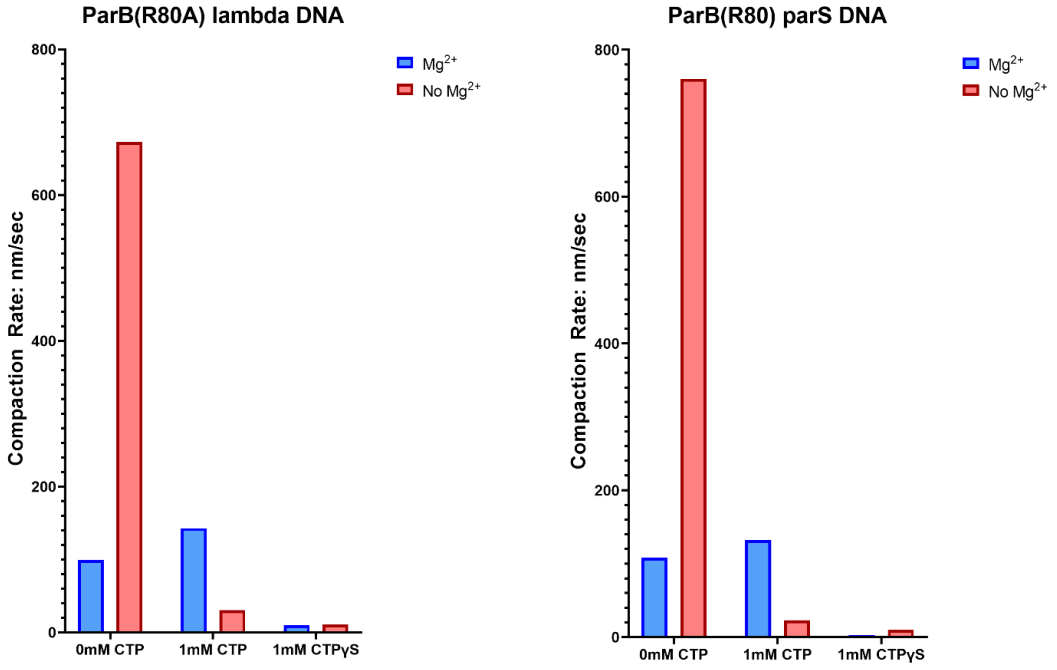

Figure 3. Overall results of untagged ParB(R80A) with Mg^{2+} ions either present or absent from buffer conditions on bacteriophage lambda DNA and lambda DNA containing a single *parS* site, in the presence of 0 mM CTP, 1 mM CTP, and 1 mM CTPγS

Cy3-labeled ParB(WT) and ParB(R80A)

Preliminary results show that non-specifically labeling both ParB(WT) and ParB(R80A) with a fluorescent Cyanine3 NHS ester (an analog of Cy3 NHS ester) does not appear to impact ParB's ability to bind lambda DNA or lambda DNA containing a single *parS* site. Compaction rates appear to be consistent with the unlabeled protein experiments based on visual observation, but more detailed analysis needs to be done. Especially, the integrated fluorescence intensity on a DNA will be translated into a rough number of BsParB protein on the DNA

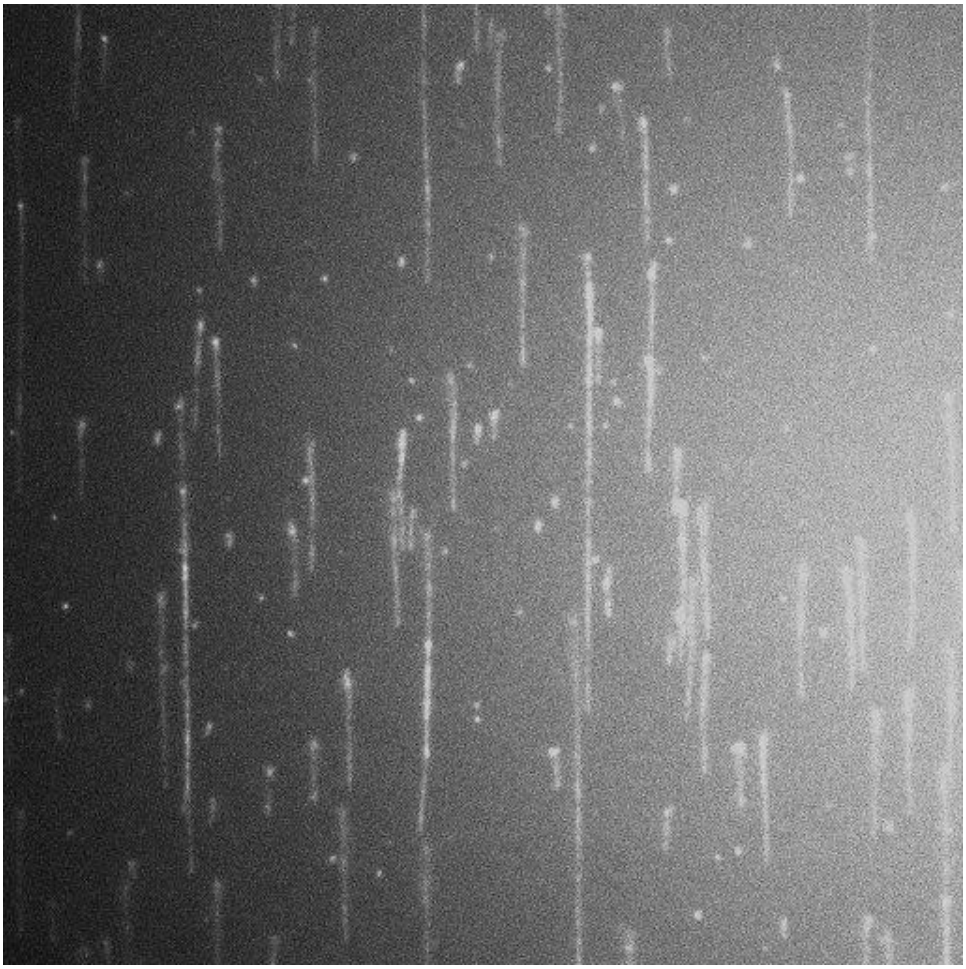

Figure 22. A snapshot image from a feasibility study with 30 nM fluorescently-labeled wildtype BsParB on lambda DNA. To reduce nonspecific protein binding to the flowcell surface, the ParB100 buffer was supplemented with 0.2 mg/mL BSA and 0.05X casein (Vector laboratories, SP-5020-250).

CHAPTER IV

SUMMARY AND CONCLUSIONS

We compared our three wildtype ParB proteins (ParB(WT), ParB(KCK-WT) and ParB(WT-KCK)) at a 50 nM concentration, and we tested them on both bacteriophage lambda DNA and lambda DNA containing a single *parS* site in the middle. CTP and CTPγS were added in a 1 mM concentration. The general trend when adding CTP and CTPγS was that the compaction rates slowed down on both lambda DNA and *parS* DNA for all three wildtype proteins.

For the untagged ParB(WT) with no CTP present, compaction was quite fast, but the addition of a *parS* site to bacteriophage lambda DNA slowed down the compaction rate by 26.8%. CTP binding and hydrolysis has been shown to be necessary for ParB disengagement from the *parS* site while the *parS* site has a higher affinity for ParB than non-specific DNA (5, 11, 33, 39), so adding a *parS* site with no CTP could explain this slower compaction rate. Adding 1 mM CTP to the untagged ParB(WT) on lambda DNA did not abolish compaction but rather slowed it down by 97.0%. Adding 1 mM CTPγS slowed down the compaction rate to 11.87 nm/sec on lambda DNA, which is a 99.3% decrease in compaction speed. This indicated that CTP hydrolysis is necessary for compaction in the ParB(WT). The non-hydrolysable CTPγS condition having the slowest compaction rate on lambda DNA makes sense with the NTDs of the

ParB dimer engaging and closing in a CTP-dependent fashion before they could load onto the DNA target, leaving very few open-ringed ParB available to load onto the DNA.

Compaction for both 1 mM CTP and 1 mM CTPγS conditions was faster on *parS* DNA than that their lambda DNA counterparts (49.4% and 119.6% increase in compaction rates, respectively), which is perhaps due to the effect of *parS* DNA having some sort of catalyzation effect on the CTP-hydrolysis dependent DNA compaction by ParB, even with the non-hydrolysable analog CTPγS. The addition of 1 mM CTP and 1 mM CTPγS to the untagged wildtype on *parS* DNA slowed down the compaction rates by 93.9% and 98.0%, respectively when compared to the 0 mM CTP condition.

Adding a KCK tag on the N-terminus of the WT (ParB(KCK-WT)) produced a dramatic effect in that it caused the compaction rate to be not as severely affected by the presence of 1 mM CTP when compared to the untagged wildtype, with the ParB(KCK-WT) on lambda DNA being faster by 808.3% and the ParB(KCK-WT) on *parS* DNA being 394.8% faster than their untagged counterpart. This pattern was the same for the 1 mM CTPγS, where ParB(KCK-WT) was 2,013.7% faster on lambda DNA and 585.5% faster on *parS* DNA than their untagged counterparts. Consistent with prior research that showed that a KCK tag did not inhibit foci formation in vivo (15), the N-terminal KCK tag did not inhibit DNA binding or compaction in vitro, but surprisingly did affect the compaction rates. This is possibly because the CTP binding pocket residing in the NTD was affected by the presence of the amino acid tag. The addition of a *parS* site on the lambda DNA did have an effect in slowing down the compaction rates of the N-terminally tagged wildtype, but how the addition of an amino acid tag effects the specific DNA binding ability is not known.

Adding a KCK tag on the C-terminus of the wildtype produced interesting results as well. In the 0 mM CTP condition on lambda DNA, the compaction rate of ParB(WT-KCK) was not significantly different to the untagged wildtype on lambda DNA- (p-value 0.3138), nor are the compaction rates of ParB(WT-KCK) on lambda DNA vs. *parS* DNA significantly different (p-value 0.2202). The KCK tag on the C-terminus increased the compaction rate compared to the untagged WT in both 1 mM CTP and 1 mM CTPγS conditions, but without a consistent pattern like ParB(KCK-WT). The 1 mM CTP conditions on both lambda DNA and *parS* DNA were not as fast as the N-terminally tagged wildtype, but still showed an increase in compaction rates at 521.0% faster on lambda DNA and 244.6% faster on *parS* DNA than their untagged wildtype counterparts. The 1 mM CTPγS conditions on both lambda DNA and *parS* DNA was still very slow and did not show full compaction in the time frame tested, with the increase in compaction rates being 78.1% faster on lambda DNA and 99.5% faster on *parS* DNA than their untagged wildtype counterparts. These data have many possible explanations, one being that the amino acid tag on the C-terminus may be not be influencing the non-specific DNA binding ability of the wildtype in any currently observable manner, and that the addition of a *parS* site does not seem to affect non-specific DNA binding either of the tagged ParB(WT-KCK) in the absence of CTP. The CTP hydrolysis-dependent activities of the wildtype may also be affected by the C-terminus KCK tag.

We also tested the effect of varying the concentration of ParB on the untagged ParB(WT) and found a generally consistent pattern that increasing protein concentration yielded faster compaction rates. For the 0 mM CTP condition, *parS* DNA generally slowed the compaction rates. Adding CTP slowed compaction rates, and CTPγS slowed them even more. For the CTP and CTPγS conditions, the addition of a *parS* site rescued the compaction rates somewhat, likely

due to the *parS*-induced increased in the CTP hydrolysis rate. Surprisingly, for the 1 mM CTPγS on *parS* DNA condition, the 30 nM was faster than the 50 nM concentration, but that were not statistically significant (p-value 0.6118), which may point to a potential maximum amount of protein being able to interact with the DNA, at which there would be a concentration reached that would no longer produce an increase in compaction rate.

We also tested the R80A mutant, using an untagged version, a KCK tag on the N-terminus, and a C-terminally appended KCK tag (ParB(R80A), ParB(KCK-R80A) and ParB(R80A-KCK), respectively. For the untagged R80A, compaction was quite slow in all CTP conditions tested (0 mM CTP, 1 mM CTP and 1 mM CTPγS), and adding a *parS* site did not seem to affect the compaction rate like in the untagged wildtype for 0 mM and 1 mM CTP. For the untagged R80A with 0 mM CTP, the compaction rate only increased by 9.05% with the addition of a *parS* site, which was not significantly different (p-value 0.5367). With 1 mM CTP, the compaction rate decreased by 7.49% with the addition of a *parS* site, which was also not significantly different (p-value 0.7016).

With 1 mM CTPγS, the DNA compaction rate of the untagged R80A protein decreased by 48.1% with the addition of a *parS* site when compared to compaction on lambda DNA with no *parS* site, which was statistically significant. This possibly implies that the untagged R80A mutant lost the ability of distinguishing between specific *parS* sequence in DNA and random sequences involved in non-specific binding, regardless of whether or not CTP is present. The significant difference for the 1 mM CTPγS condition could point to the fact that *parS*-catalyzed CTP hydrolysis is still important for compaction. Even though the compaction by untagged R80A was slow, it was not zero for the 0 mM and 1 mM CTP conditions. This contradicts previous reports that the R80A mutant does not compact DNA or bind to CTP. Adding CTPγS

did appear to abolish all compaction in the untagged R80A mutant, which also indicates that CTP definitely does bind to the mutant R80A.

The real interesting data is the N-terminus KCK-tagged protein, which shows a drastic increase in compaction rates for all CTP conditions tested and on both lambda DNA and *parS* DNA, likely caused by adding a KCK tag to the N-terminus of the NTD, which has the CTP binding domain with the R80 residue contacting the β-phosphate of CTP. The addition of an N-terminally appended KCK tag for the 0 mM, 1 mM CTP and 1 mM CTPγS conditions on lambda DNA caused the compaction rate to increase by 503.6%, 226.2% and 7,337.7%, respectively, compared to the untagged R80A. On *parS* DNA, the 0 mM, 1 mM CTP and 1 mM CTPγS conditions for ParB(KCK-R80A) on *parS* DNA had compaction rates that increased by 925.8%, 840.2% and 3346.0%, respectively, compared to the untagged R80A. There is no consistent pattern for ParB(KCK-R80A) compaction rates on lambda DNA vs. *parS* DNA for all CTP conditions tested. How the addition of a KCK tag affects DNA compaction and how that compaction is affected by CTP binding and hydrolysis are not understood.

Also, the C-terminus KCK tagged R80A mutant shows very different results to the untagged R80A, with the general pattern showing faster compaction that the untagged R80A. On *parS* DNA, ParB(R80A-KCK) shows a decreasing pattern in the compaction rate with the addition of 1 mM CTP and 1 mM CTPγS, much like all three tagged versions of the wildtype. The most surprising finding for ParB(R80A-KCK) was that on lambda DNA, all three CTP conditions had nearly identical compactions rates; 677.8, 677.3 and 674.3 nm/sec on 0 mM, 1 mM CTP and 1 mM CTPγS, respectively, and none were significantly different from each other (p-values 0.9946 for 0 mM CTP vs 1 mM CTP, 0.9709 for 1 mM CTP vs 1 mM CTPγS, 0.9693 for 0 mM CTP vs 1 mM CTPγS). With 0 mM CTP added, the compaction rates between

ParB(R80A-KCK) on lambda vs. *parS* DNA are not significantly different (p-value 0.1462), nor are they significantly different with 1 mM CTP on lambda vs. *parS* DNA (p-value 0.4029). For 1 mM CTPγS, the compaction rates between lambda and *parS* DNA are significantly different, with the compaction rate decreasing by 88.4% with the addition of the *parS* site.

Since Mg^{2+} ions were found to influence specific and non-specific binding in ParB as well as coordinate with the triphosphate moiety of CTP, we decided to test what removing Mg^{2+} ions would do to the compaction rate of the untagged R80A mutant (15). These conditions were tested at the 50 nM protein concentration and 1 mM CTP or CTPγS. Surprisingly, the mutant compacted DNA the fastest with no Mg^{2+} ions present with no CTP present, but the lack of Mg^{2+} ions slow down compaction in the CTP condition. Mg^{2+} ions likely interact with both the protein and with the triphosphate moiety of CTP. Our hypothesized theory on why previous researchers showed no compaction, no foci formation and no CTP binding in the R80A mutant is that the conditions tested were likely what I have highlighted here: no Mg^{2+} ions in the buffer and CTP likely co-purified with the protein. We treated our protein with apyrase to deplete any CTP that may have been co-purified.

Overall, adding 1 mM CTP and 1 mM CTPγS does impact ParB-mediated DNA compaction, and the addition of a *parS* site also modulates this compaction in the wildtype, with the implication that CTP hydrolysis is required for faster compaction and hydrolysis can be stimulated by the presence of a single *parS* site on bacteriophage lambda DNA. It would be interesting to see how adding more *parS* sites to the lambda DNA would impact the compaction rates of the proteins tested. For the NTD, which contains the CTP-binding pocket, adding a KCK tag seems to modulate wildtype protein compaction by increasing it, even in the presence of 1

mM CTP and 1 mM CTPγS, but the mechanism is not known yet. Adding a KCK tag to the CTD likely influences the non-specific binding ability of ParB, but how is not yet known.

For ParB(R80A), we saw results that contradicted previous reports that the R80A recombinant mutant does not compact DNA and does not bind to CTP, since CTPγS abolished DNA compaction this implies that CTP does bind to the protein. Again, adding a KCK tag to the NTD produced large increases in the compaction rate of the mutant protein, likely because the NTD does contain the CTP binding pocket. Mg^{2+} ions seem to be necessary for DNA compaction when CTP is present, and at least for the untagged R80A, adding a single *parS* site does not seem to make a difference in the compaction rate. Again, seeing multiple *parS* sites engineered on the lambda DNA would be an interesting experiment in how it would impact compaction rates.

The findings on terminally appending a lysine-cysteine-lysine (KCK) tag to the ParB protein should be of interest since the tags, either on the N-terminus or C-terminus, seem to have a significant impact on the DNA compacting activity of both the wildtype ParB and mutant R80A ParB. While this tag does not seem to inhibit gross protein localization and foci formation for in vivo experiments, adding addition amino acids to areas of the protein that have key functions in the protein's dimerization activity and DNA binding can have an unintended impact on any experiments using these tagged proteins.

REFERENCES

Antar, H., Soh, Y.-M., Zamuer, S., Bock, F. P., Anchimiuk, A., De Los Rios, P., & Gruber, S. (2021). Relief of parb autoinhibition by Pars DNA catalysis and parb recycling by CTP hydrolysis promote bacterial centromere assembly. Science Advances, 7, 1–17. https://doi.org/10.1101/2021.05.05.442573

Autret, S., Nair, R., & Errington, J. (2001). Genetic analysis of the chromosome segregation protein spo0j of bacillus subtilis: Evidence for separate domains involved in DNA binding and interactions with Soj protein. Molecular Microbiology, 41(3), 743–755. https://doi.org/10.1046/j.1365-2958.2001.02551.x

Barillà, D., Rosenberg, M. F., Nobbmann, U., & Hayes, F. (2005). Bacterial DNA segregation dynamics mediated by the polymerizing protein parf. The EMBO Journal, 24(7), 1453–1464. https://doi.org/10.1038/sj.emboj.7600619

Basu, M. K., & Koonin, E. V. (2005). Evolution of eukaryotic cysteine sulfinic acid reductase, sulfiredoxin (SRX), from bacterial chromosome partitioning protein parb. Cell Cycle, 4(7), 947–952. https://doi.org/10.4161/cc.4.7.1786

Bouet, J.-Y., Surtees, J. A., & Funnell, B. E. (2000). Stoichiometry of P1 plasmid partition complexes. Journal of Biological Chemistry, 275(11), 8213–8219. https://doi.org/10.1074/jbc.275.11.8213

Breier, A. M., & Grossman, A. D. (2007). Whole-genome analysis of the chromosome partitioning and sporulation protein spo0j (parb) reveals spreading and origin-distal sites on the bacillus subtilis chromosome. Molecular Microbiology, 64(3), 703–718. https://doi.org/10.1111/j.1365-2958.2007.05690.x

Broedersz, C. P., Wang, X., Meir, Y., Loparo, J. J., Rudner, D. Z., & Wingreen, N. S. (2014). Condensation and localization of the partitioning protein parb on the bacterial chromosome. Proceedings of the National Academy of Sciences, 111(24), 8809–8814. https://doi.org/10.1073/pnas.1402529111

Chen, B.-W., Lin, M.-H., Chu, C.-H., Hsu, C.-E., & Sun, Y.-J. (2015). Insights into parb spreading from the complex structure of SPO0J and pars. Proceedings of the National Academy of Sciences, 112(21), 6613–6618. https://doi.org/10.1073/pnas.1421927112

Davis, M. A., Martin, K. A., & Austin, S. J. (1992). Biochemical activities of the para partition protein of the P1 plasmid. Molecular Microbiology, 6(9), 1141–1147. https://doi.org/10.1111/j.1365-2958.1992.tb01552.x

de Balaguer, F., Aicart-Ramos, C., Fisher, G. L. M., de Bragança, S., Martin-Cuevas, E. M., Pastrana, C. L., Dillingham, M. S., & Moreno-Herrero, F. (2021). CTP promotes efficient parb-dependent DNA condensation by facilitating one-dimensional diffusion from Pars. ELife, 10. https://doi.org/10.7554/elife.67554

Debaugny, R. E., Sanchez, A., Rech, J., Labourdette, D., Dorignac, J., Geniet, F., Palmeri, J., Parmeggiani, A., Boudsocq, F., Anton Leberre, V., Walter, J. C., & Bouet, J. Y. (2018). A conserved mechanism drives partition complex assembly on bacterial chromosomes and plasmids. Molecular Systems Biology, 14(11). https://doi.org/10.15252/msb.20188516

Fish, K. N. (2009). Total internal reflection fluorescence (TIRF) microscopy. Current Protocols in Cytometry, 50(1). https://doi.org/10.1002/0471142956.cy1218s50

Fisher, G. L. M., Pastrana, C. L., Higman, V. A., Koh, A., Taylor, J. A., Butterer, A., Craggs, T., Sobott, F., Murray, H., Crump, M. P., Moreno-Herrero, F., & Dillingham, M. S. (2017). The structural basis for dynamic DNA binding and bridging interactions which condense the bacterial centromere. ELife, 6. https://doi.org/10.7554/elife.28086

Gerdes, K., Howard, M., & Szardenings, F. (2010). Pushing and pulling in prokaryotic DNA segregation. Cell, 141(6), 927–942. https://doi.org/10.1016/j.cell.2010.05.033

Graham, T. G. W., Wang, X., Song, D., Etson, C. M., van Oijen, A. M., Rudner, D. Z., & Loparo, J. J. (2014). PARB spreading requires DNA bridging. Genes & Development, 28(11), 1228–1238. https://doi.org/10.1101/gad.242206.114

Hammar, P., Leroy, P., Mahmutovic, A., Marklund, E. G., Berg, O. G., & Elf, J. (2012). The lac repressor displays facilitated diffusion in living cells. Science, 336(6088), 1595–1598. https://doi.org/10.1126/science.1221648

Hayes, F., & Barillà, D. (2006). The bacterial segrosome: A dynamic nucleoprotein machine for DNA trafficking and segregation. Nature Reviews Microbiology, 4(2), 133–143. https://doi.org/10.1038/nrmicro1342

Hui, M. P., Galkin, V. E., Yu, X., Stasiak, A. Z., Stasiak, A., Waldor, M. K., & Egelman, E. H. (2010). Para2, a vibrio cholerae chromosome partitioning protein, forms left-handed helical filaments on DNA. Proceedings of the National Academy of Sciences, 107(10), 4590–4595. https://doi.org/10.1073/pnas.0913060107

Jalal, A. S. B., Tran, N. T., & Le, T. B. K. (2020). PARB spreading on DNA requires cytidine triphosphate in vitro. ELife, 9. https://doi.org/10.7554/elife.53515

Jönsson, T. J., Murray, M. S., Johnson, L. C., & Lowther, W. T. (2008). Reduction of cysteine sulfinic acid in peroxiredoxin by sulfiredoxin proceeds directly through a sulfinic phosphoryl ester intermediate. Journal of Biological Chemistry, 283(35), 23846–23851. https://doi.org/10.1074/jbc.m803244200

Le Gall, A., Cattoni, D. I., Guilhas, B., Mathieu-Demazière, C., Oudjedi, L., Fiche, J.-B., Rech, J., Abrahamsson, S., Murray, H., Bouet, J.-Y., & Nollmann, M. (2016). Bacterial partition complexes segregate within the volume of the nucleoid. Nature Communications, 7(1). https://doi.org/10.1038/ncomms12107

Leonard, T. A., Butler, P. J., & Löwe, J. (2004). Structural analysis of the chromosome segregation protein spo0j from Thermus thermophilus. Molecular Microbiology, 53(2), 419–432. https://doi.org/10.1111/j.1365-2958.2004.04133.x

Lim, H. C., Surovtsev, I. V., Beltran, B. G., Huang, F., Bewersdorf, J., & Jacobs-Wagner, C. (2014). Evidence for a DNA-relay mechanism in parabs-mediated chromosome segregation. ELife, 3. https://doi.org/10.7554/elife.02758

Lin, D. C.-H., & Grossman, A. D. (1998). Identification and characterization of a bacterial chromosome partitioning site. Cell, 92(5), 675–685. https://doi.org/10.1016/s0092-8674(00)81135-6

Lin, L., Osorio Valeriano, M., Harms, A., Søgaard-Andersen, L., & Thanbichler, M. (2017). Bactofilin-mediated organization of the parabs chromosome segregation system in Myxococcus Xanthus. Nature Communications, 8(1). https://doi.org/10.1038/s41467-017-02015-z

Lynch, A. S., & Wang, J. C. (1995). SOPB protein-mediated silencing of genes linked to the sopc locus of escherichia coli F plasmid. Proceedings of the National Academy of Sciences, 92(6), 1896–1900. https://doi.org/10.1073/pnas.92.6.1896

Madariaga-Marcos, J., Pastrana, C. L., Fisher, G. L. M., Dillingham, M. S., & Moreno-Herrero, F. (2019). PARB dynamics and the critical role of the CTD in DNA condensation unveiled by combined force-fluorescence measurements. ELife, 8. https://doi.org/10.7554/elife.43812

Murray, H., Ferreira, H., & Errington, J. (2006). The bacterial chromosome segregation protein spo0j spreads along DNA from pars nucleation sites. Molecular Microbiology, 61(5), 1352–1361. https://doi.org/10.1111/j.1365-2958.2006.05316.x

Osorio-Valeriano, M., Altegoer, F., Steinchen, W., Urban, S., Liu, Y., Bange, G., & Thanbichler, M. (2019). ParB-type DNA segregation proteins are CTP-dependent molecular switches. Cell, 179(7). https://doi.org/10.1016/j.cell.2019.11.015

Ptacin, J. L., Lee, S. F., Garner, E. C., Toro, E., Eckart, M., Comolli, L. R., Moerner, W. E., & Shapiro, L. (2010). A spindle-like apparatus guides bacterial chromosome segregation. Nature Cell Biology, 12(8), 791–798. https://doi.org/10.1038/ncb2083

Rodionov, O., Łobocka, M., & Yarmolinsky, M. (1999). Silencing of genes flanking the P1 plasmid centromere. Science, 283(5401), 546–549. https://doi.org/10.1126/science.283.5401.546

Sanchez, A., Rech, J., Gasc, C., & Bouet, J.-Y. (2013). Insight into centromere-binding properties of parb proteins: A secondary binding motif is essential for bacterial genome maintenance. Nucleic Acids Research, 41(5), 3094–3103. https://doi.org/10.1093/nar/gkt018

Sanchez, A., Cattoni, D. I., Walter, J.-C., Rech, J., Parmeggiani, A., Nollmann, M., & Bouet, J.-Y. (2015). Stochastic self-assembly of parb proteins builds the bacterial DNA segregation apparatus. Cell Systems, 1(2), 163–173. https://doi.org/10.1016/j.cels.2015.07.013

Schumacher, M. A., & Funnell, B. E. (2005). Structures of parb bound to DNA reveal mechanism of Partition Complex Formation. Nature, 438(7067), 516–519. https://doi.org/10.1038/nature04149

Schumacher, M. A., Mansoor, A., & Funnell, B. E. (2007). Structure of a four-way bridged parb-DNA complex provides insight into P1 Segrosome Assembly. Journal of Biological Chemistry, 282(14), 10456–10464. https://doi.org/10.1074/jbc.m610603200

Soh, Y.-M., Davidson, I. F., Zamuner, S., Basquin, J., Bock, F. P., Taschner, M., Veening, J.-W., De Los Rios, P., Peters, J.-M., & Gruber, S. (2019). Self-organization of pars centromeres by the parb CTP hydrolase. Science, 366(6469), 1129–1133. https://doi.org/10.1126/science.aay3965

Song, D., Rodrigues, K., Graham, T. G. W., & Loparo, J. J. (2017). A network of CIS and trans interactions is required for parb spreading. Nucleic Acids Research, 45(12), 7106–7117. https://doi.org/10.1093/nar/gkx271

Surtees, J. A., & Funnell, B. E. (2001). The DNA binding domains of P1 parb and the architecture of the P1 Plasmid Partition Complex. Journal of Biological Chemistry, 276(15), 12385–12394. https://doi.org/10.1074/jbc.m009370200

Taylor, J. A., Pastrana, C. L., Butterer, A., Pernstich, C., Gwynn, E. J., Sobott, F., Moreno-Herrero, F., & Dillingham, M. S. (2015). Specific and non-specific interactions of parb with DNA: Implications for chromosome segregation. Nucleic Acids Research, 43(2), 719–731. https://doi.org/10.1093/nar/gku1295

Vecchiarelli, A. G., Mizuuchi, K., & Funnell, B. E. (2012). Surfing biological surfaces: Exploiting the nucleoid for partition and transport in bacteria. Molecular Microbiology, 86(3), 513–523. https://doi.org/10.1111/mmi.12017

Wang, X., Brandão, H. B., Le, T. B., Laub, M. T., & Rudner, D. Z. (2017). bacillus subtilis SMC complexes juxtapose chromosome arms as they travel from origin to Terminus. Science, 355(6324), 524–527. https://doi.org/10.1126/science.aai8982

Watanabe, E., Wachi, M., Yamasaki, M., & Nagai, K. (1992). ATPase activity of SOPA, a protein essential for active partitioning of F Plasmid. Molecular and General Genetics MGG, 234(3), 346–352. https://doi.org/10.1007/bf00538693

Wilhelm, L., Bürmann, F., Minnen, A., Shin, H.-C., Toseland, C. P., Oh, B.-H., & Gruber, S. (2015). SMC condensin entraps chromosomal DNA by an ATP hydrolysis dependent loading mechanism in bacillus subtilis. ELife, 4. https://doi.org/10.7554/elife.06659

Yamaichi, Y., & Niki, H. (2000). Active segregation by the Bacillus subtilis partitioning system in Escherichia coli. Proceedings of the National Academy of Sciences, 97(26), 14656–14661. https://doi.org/10.1073/pnas.97.26.14656

APPENDIX

APPENDIX

GRAPHS AND TABLES OF THE DATA

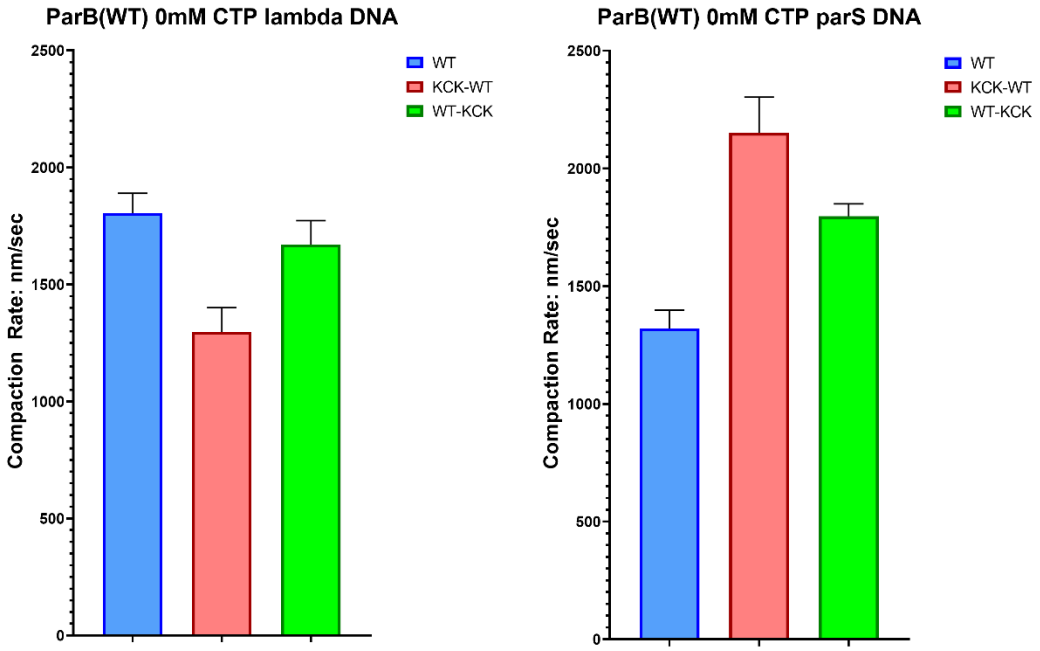

Figure 4. Comparison of tagged and untagged 50 nM ParB(WT) compaction rate of lambda and *parS* DNA in nm/sec in the presence of 0 mM CTP. Error bars represent SEM.

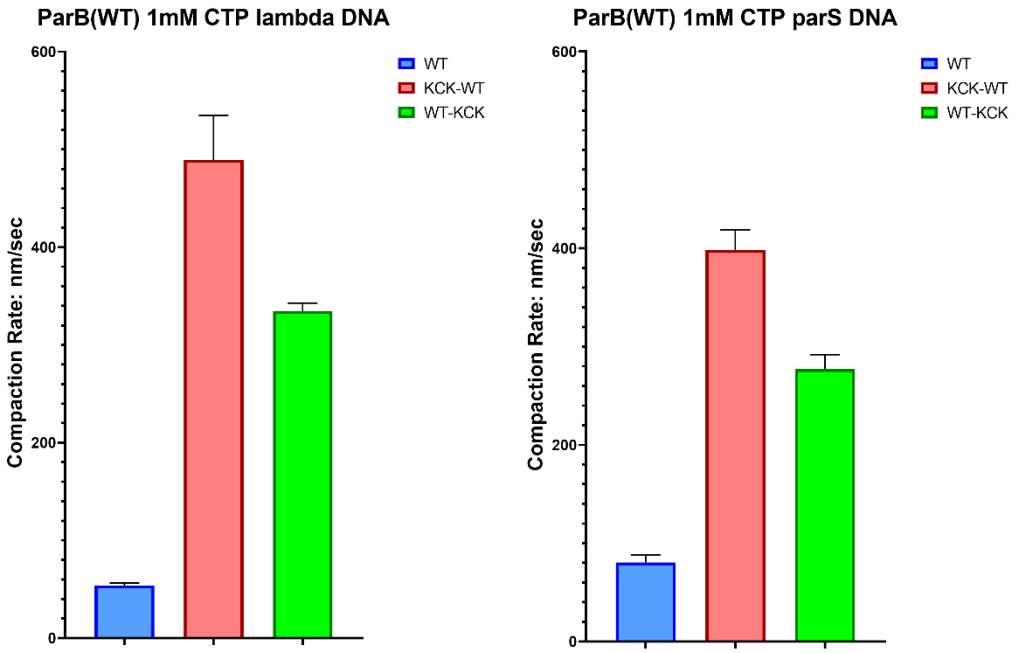

Figure 5. Comparison of tagged and untagged 50 nM ParB(WT) compaction rate of lambda and *parS* DNA in nm/sec in the presence of 1 mM CTP. Error bars represent SEM.

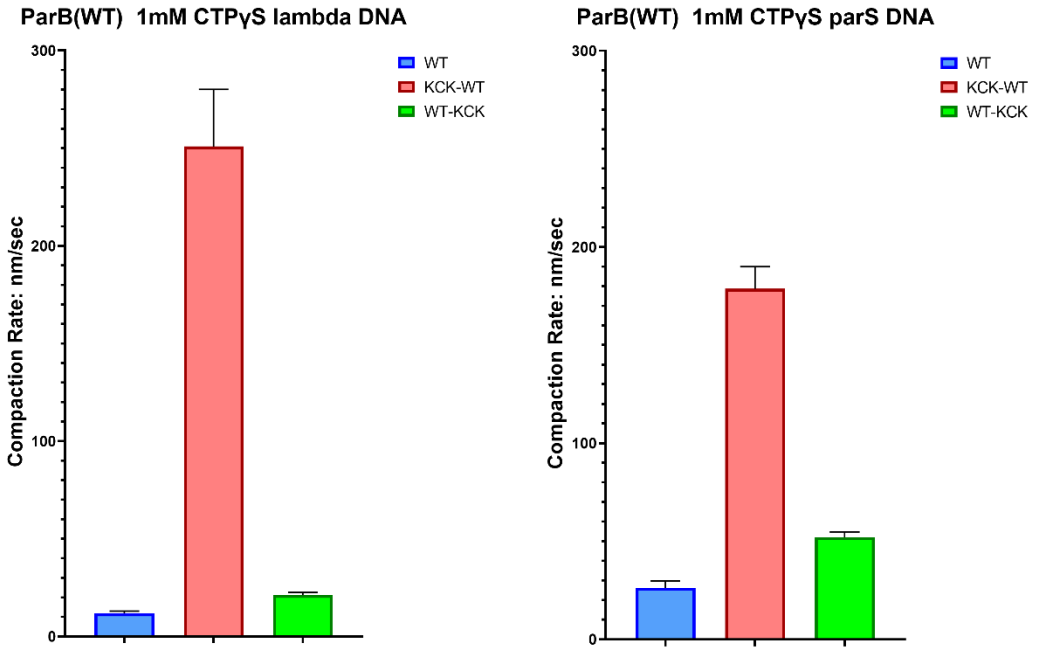

Figure 6. Comparison of tagged and untagged 50 nM ParB(WT) compaction rate of lambda and *parS* DNA in nm/sec in the presence of 1 mM CTPγS. Error bars represent SEM.

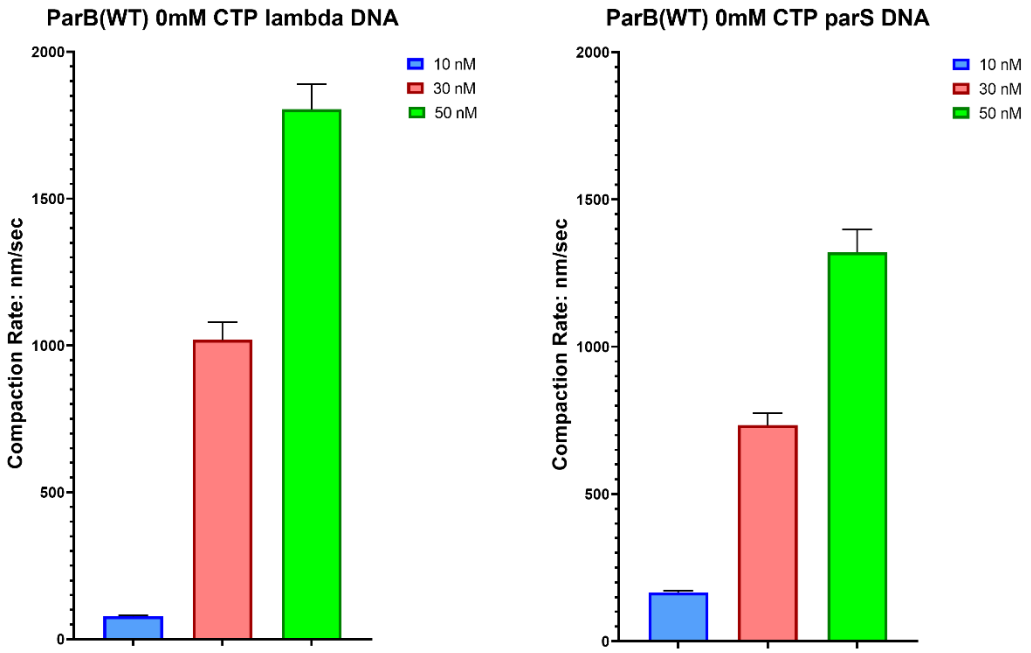

Figure 7. Comparison of 50 nM, 30 nM, and 10 nM untagged ParB(WT) compaction rate of lambda and *parS* DNA in nm/sec in the presence of 0 mM CTP. Error bars represent SEM.

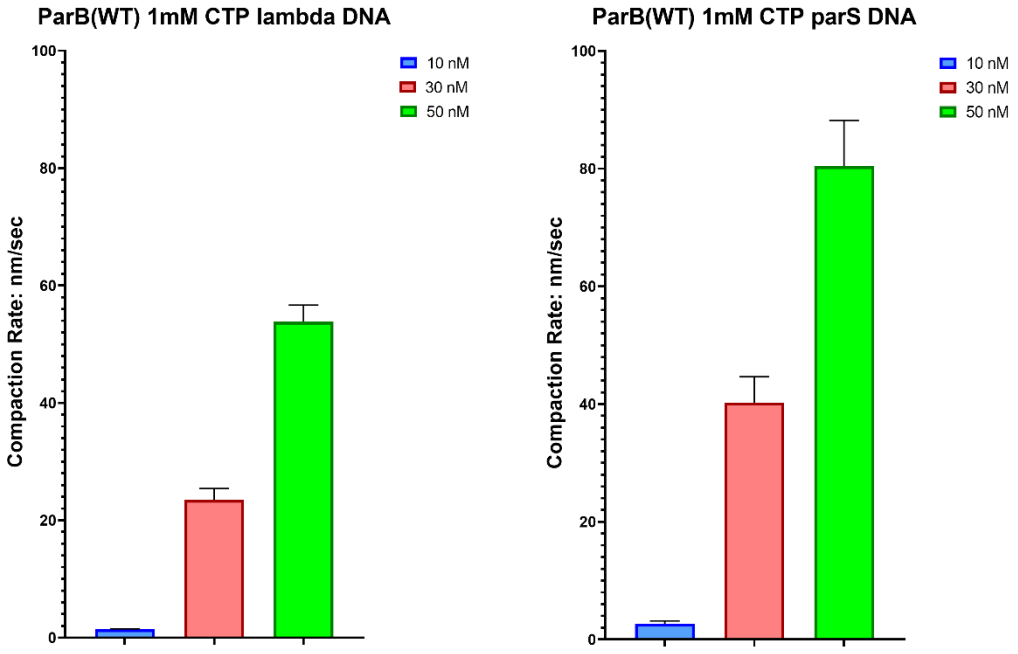

Figure 8. Comparison of 50 nM, 30 nM, and 10 nM untagged ParB(WT) compaction rate of lambda and *parS* DNA in nm/sec in the presence of 1 mM CTP. Error bars represent SEM.

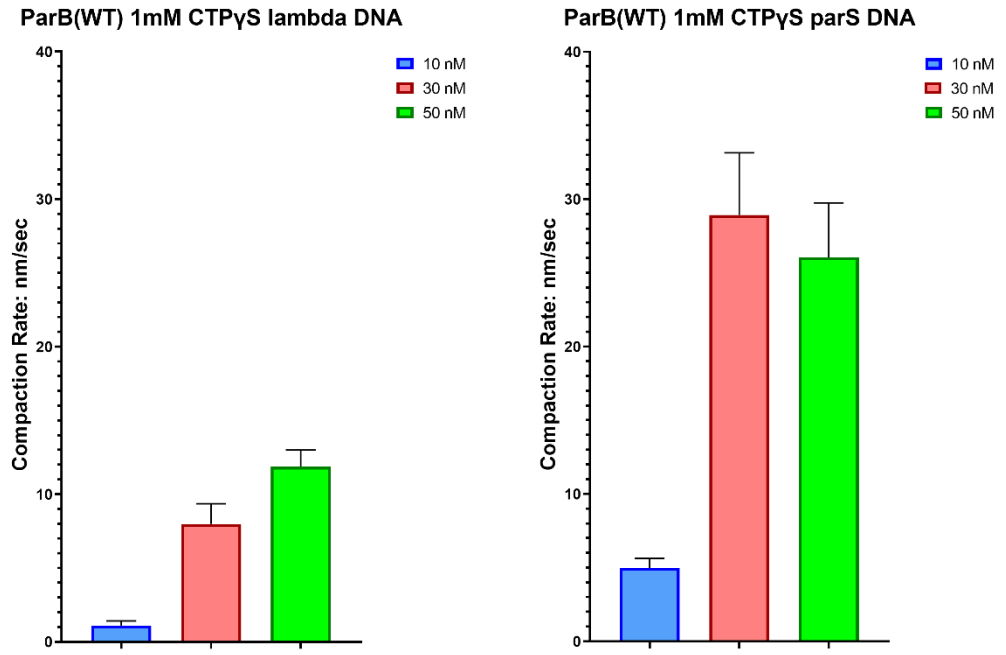

Figure 9. Comparison of 50 nM, 30 nM, and 10 nM untagged ParB(WT) compaction rate of lambda and *parS* DNA in the presence of 1 mM CTPγS. Error bars represent SEM.

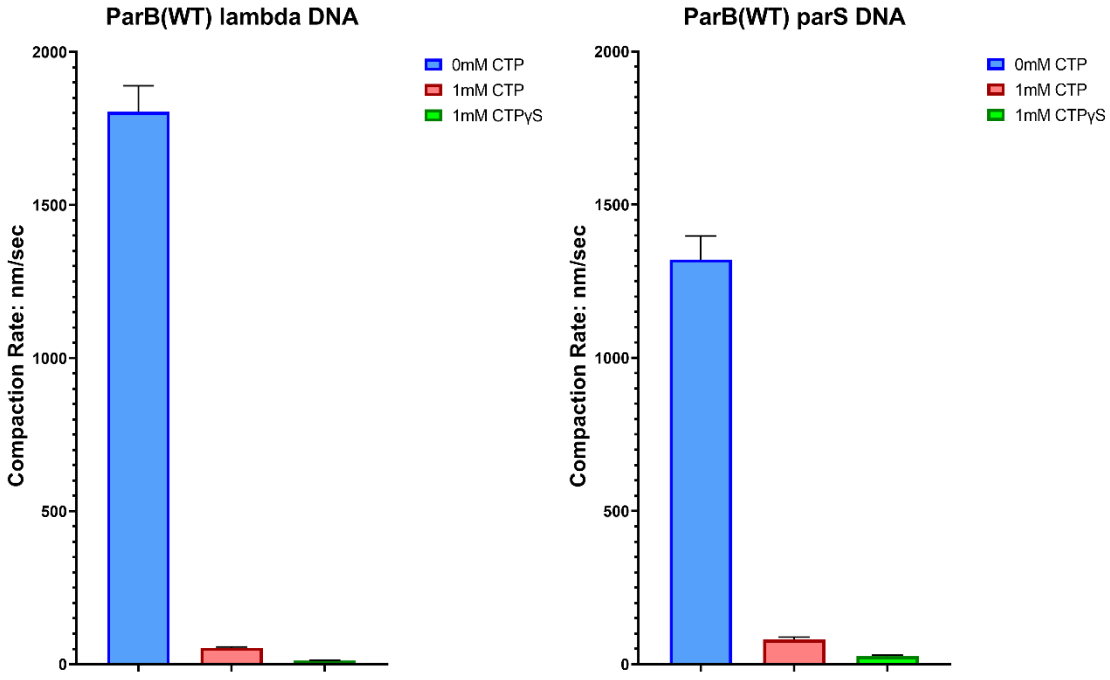

Figure 10. Untagged 50 nM ParB(WT) compaction rate of lambda and *parS* DNA in nm/sec in the presence of 0 mM CTP, 1 mM CTP, and 1 mM CTPγS. Error bars represent SEM.

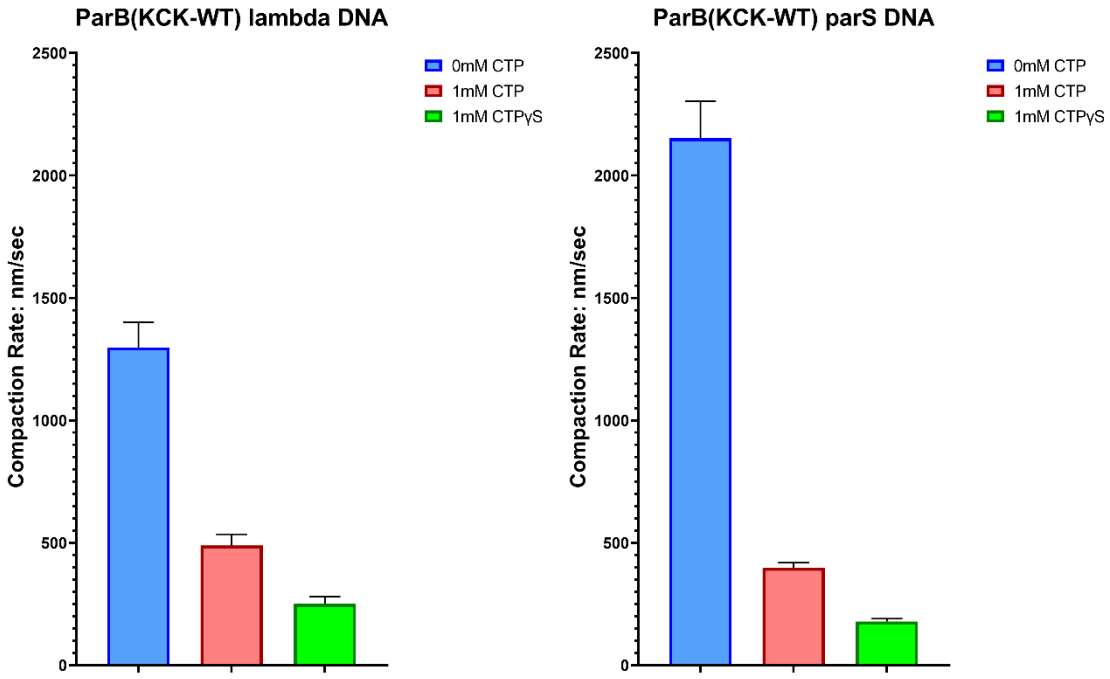

Figure 11. N-terminally tagged 50 nM ParB(KCK-WT) compaction rate of lambda and *parS* DNA in nm/sec in the presence of 0 mM CTP, 1 mM CTP, and 1 mM CTPγS. Error bars represent SEM.

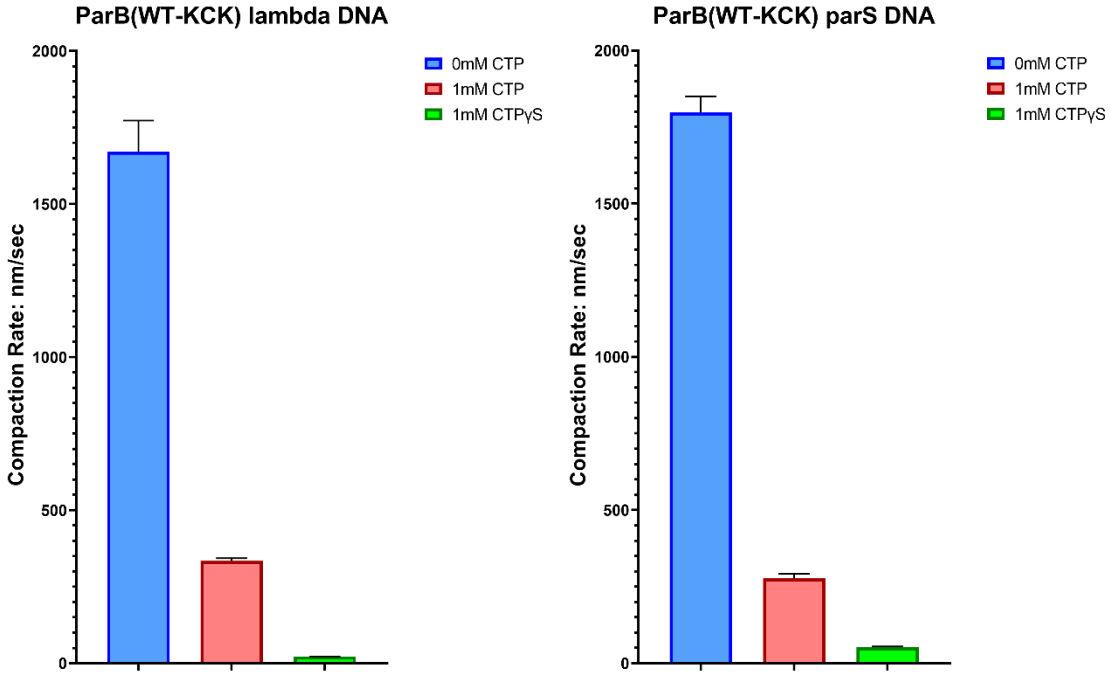

Figure 12. C-terminally tagged 50 nM ParB(WT-KCK) compaction rate of lambda and *parS* DNA in nm/sec in the presence of 0 mM CTP, 1 mM CTP, and 1 mM CTPγS. Error bars represent SEM.

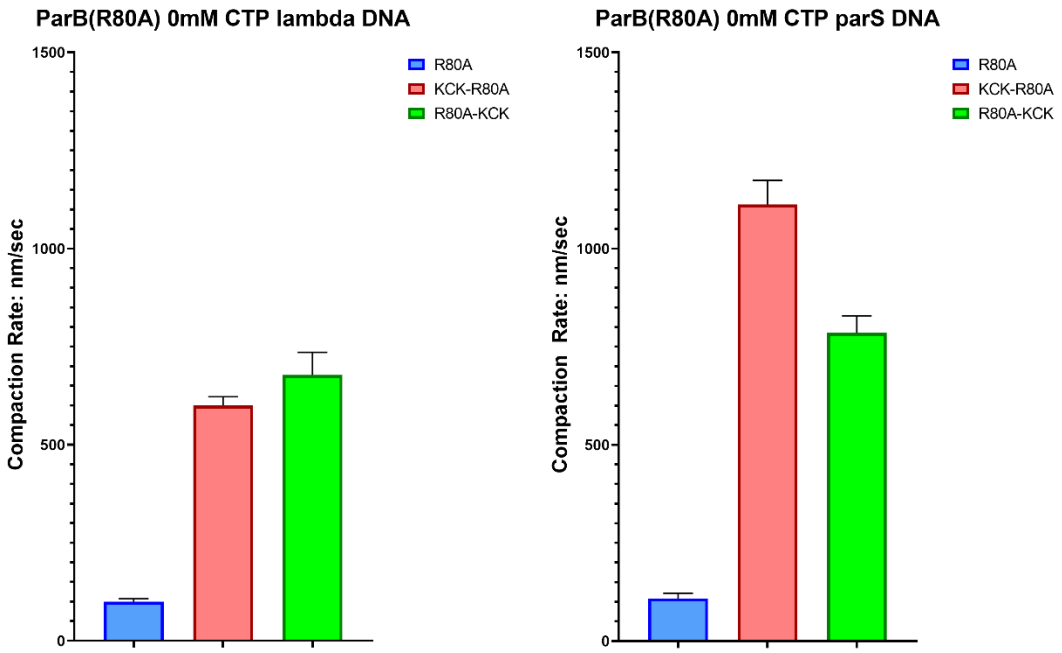

Figure 13. Comparison of tagged and untagged 50 nM ParB(R80A) compaction rate of lambda and *parS* DNA in nm/sec in the presence of 0 mM CTP. Error bars represent SEM.

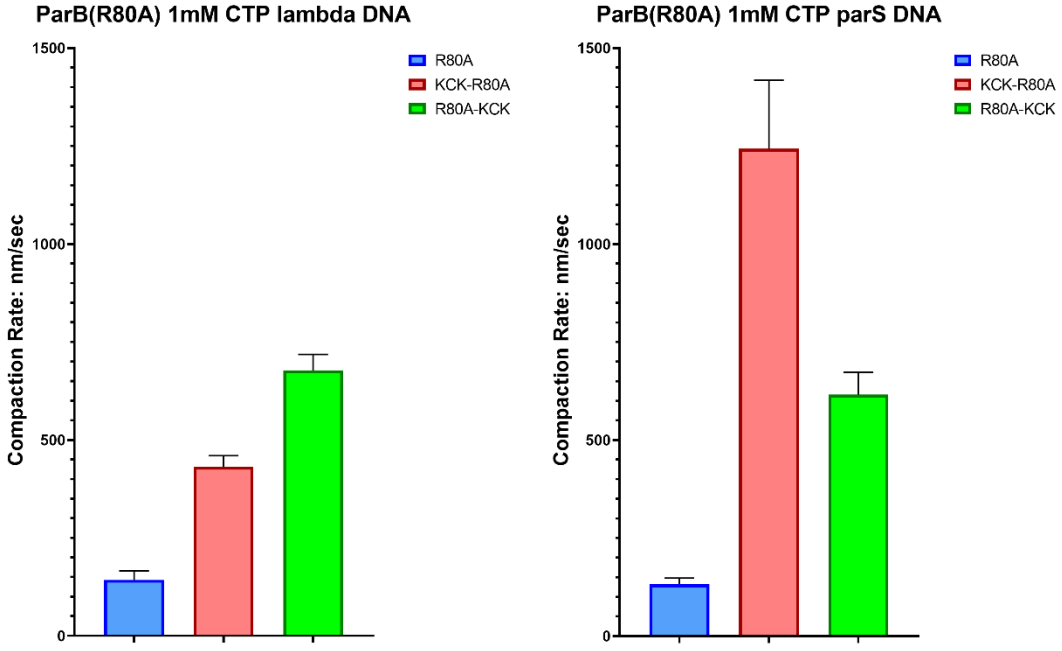

Figure 14. Comparison of tagged and untagged 50 nM ParB(R80A) compaction rate of lambda and *parS* DNA in nm/sec in the presence of 1 mM CTP. Error bars represent SEM.

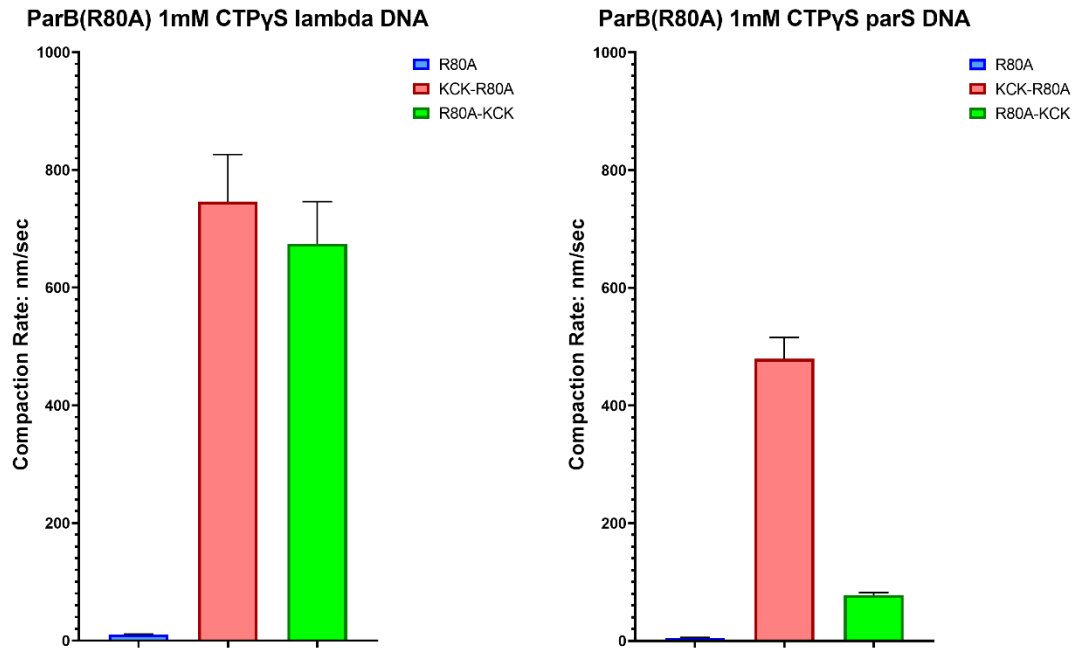

Figure 15. Comparison of tagged and untagged 50 nM ParB(R80A) compaction rate of lambda and *parS* DNA in nm/sec in the presence of 1 mM CTPγS. Error bars represent SEM.

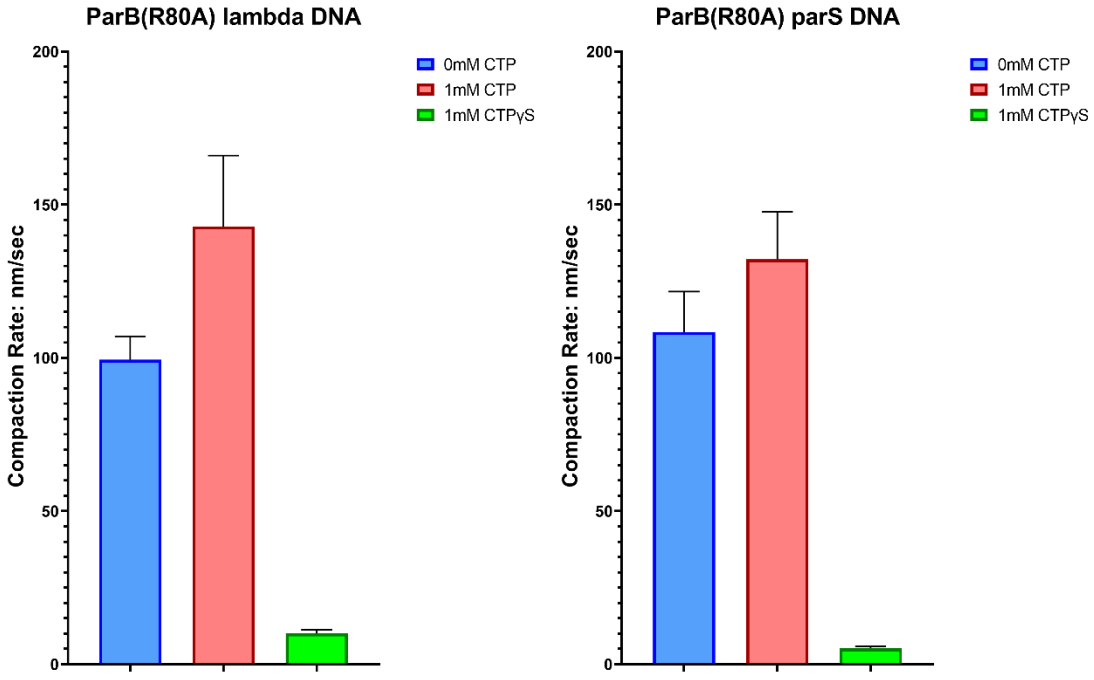

Figure 16. Untagged 50 nM ParB(R80A) compaction rate of lambda and *parS* DNA in nm/sec in the presence of 0 mM CTP, 1 mM CTP, and 1 mM CTPγS. Error bars represent SEM.

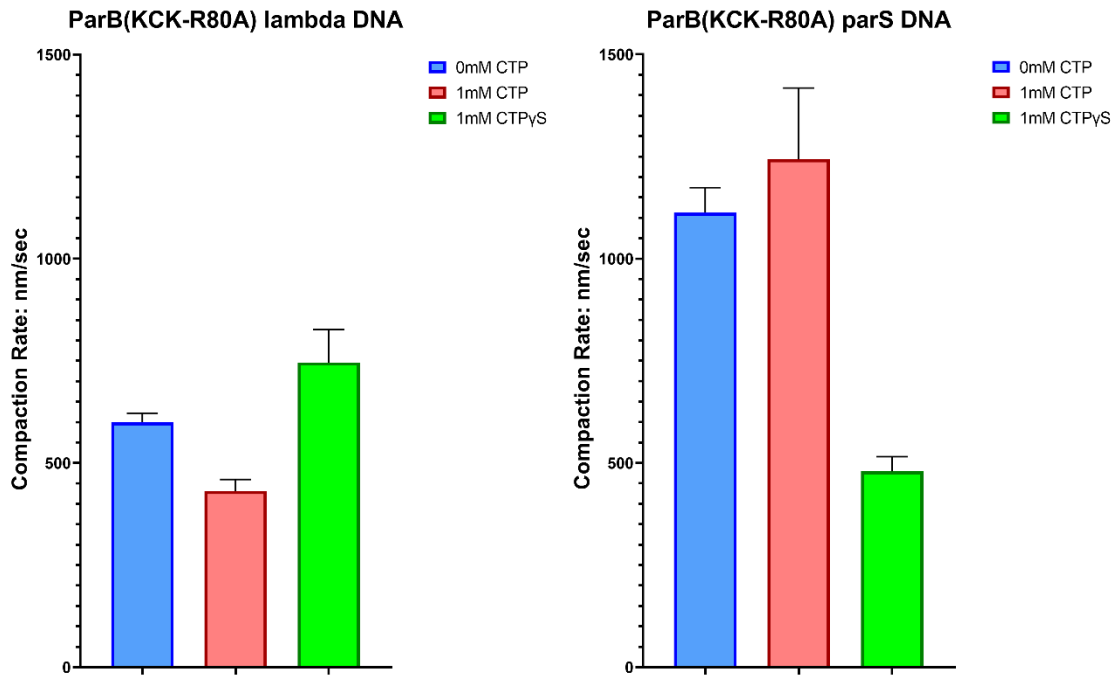

Figure 17. N-terminally tagged 50 nM ParB(KCK-R80A) compaction rate of lambda and *parS* DNA in nm/sec in the presence of 0 mM CTP, 1 mM CTP, and 1 mM CTPγS. Error bars represent SEM.

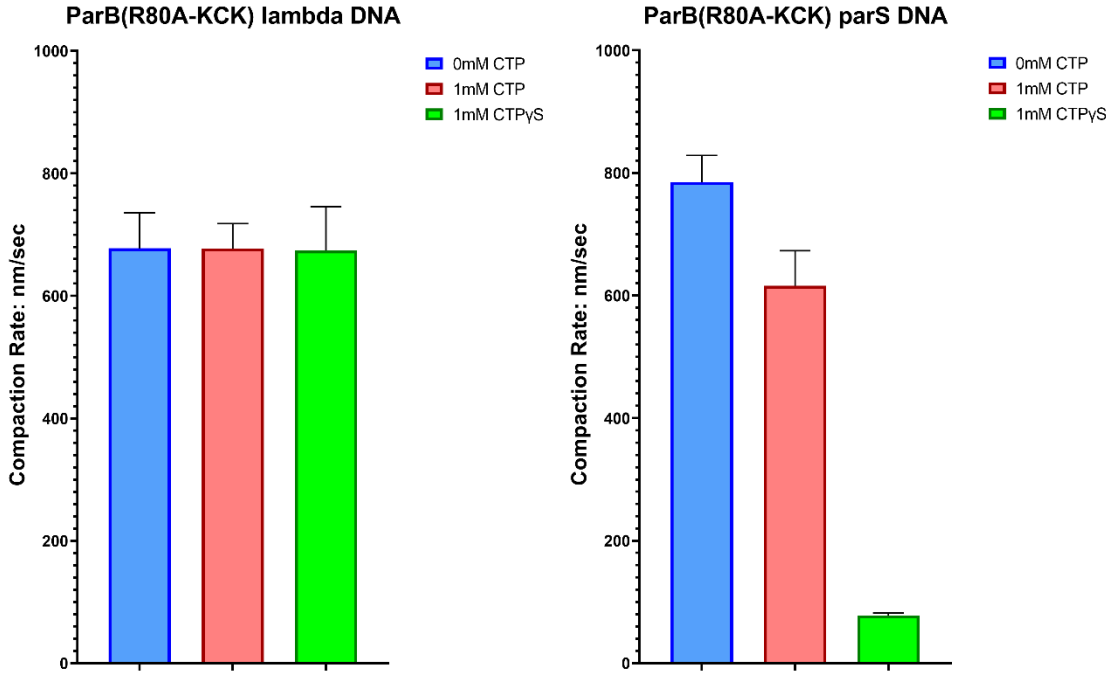

Figure 18. C-terminally tagged 50 nM ParB(R80A-KCK) compaction rate of lambda and *parS* DNA in nm/sec in the presence of 0 mM CTP, 1 mM CTP, and 1 mM CTPγS. Error bars represent SEM.

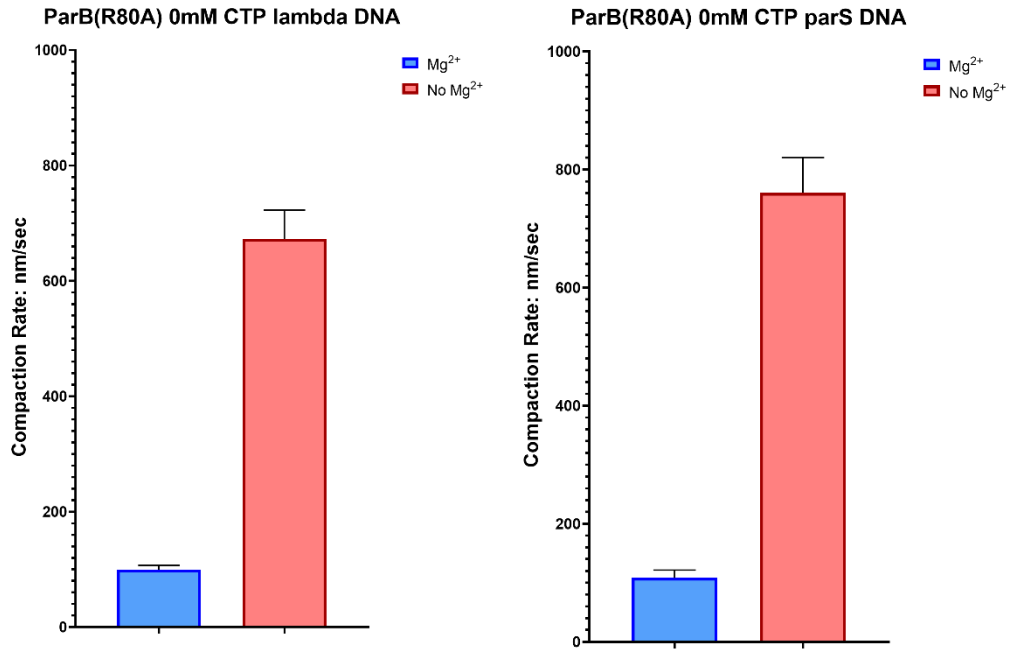

Figure 19. Comparison of untagged 50 nM ParB(R80A) compaction rate of lambda and *parS* DNA in the presence of 0 mM CTP with Mg^{2+} ions present or absent. Error bars represent SEM.

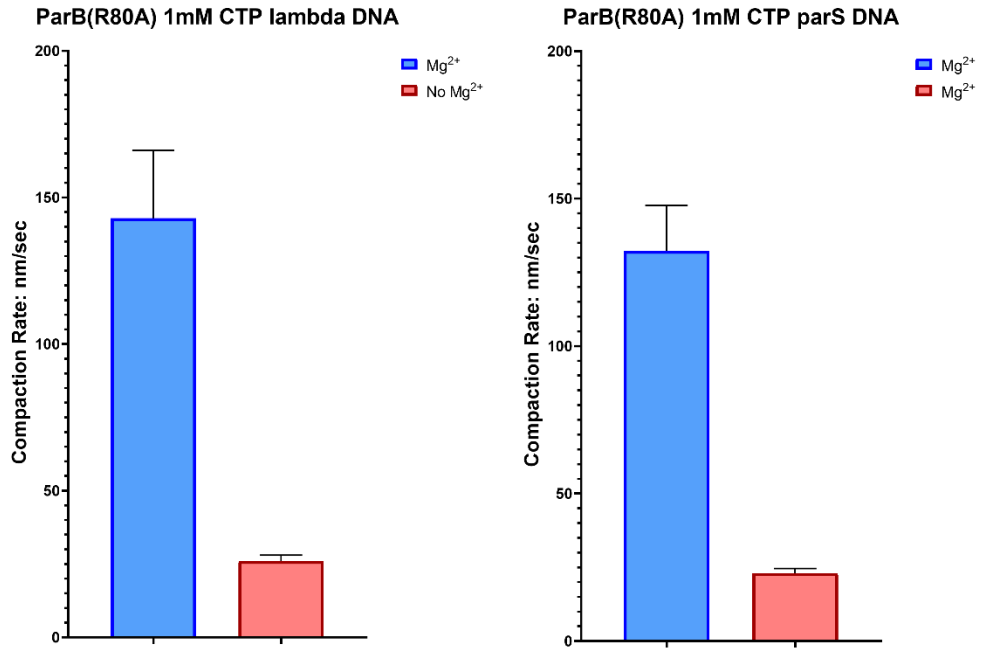

Figure 20. Comparison of untagged 50 nM ParB(R80A) compaction rate of lambda and *parS* DNA in the presence of 1 mM CTP with Mg^{2+} ions present or absent. Error bars represent SEM.

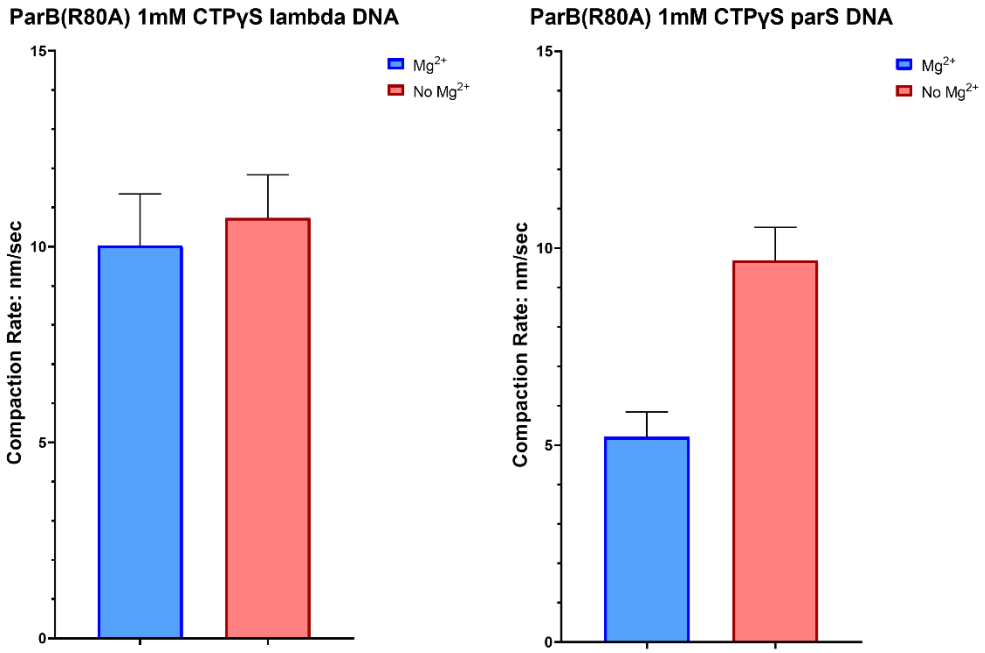

Figure 21. Comparison of untagged 50 nM ParB(R80A) compaction rate of lambda and *parS* DNA in the presence of 1 mM CTPγS with Mg^{2+} ions present or absent. Error bars represent SEM.

Table 1. Compaction rates in nm/sec for untagged and tagged ParB(WT), ParB(KCK-WT) and ParB(WT-KCK) on lambda DNA and *parS* DNA

	ParB(WT) 50 nM lambda DNA - 0 mM CTP	ParB(WT) 50 nM lambda DNA - 1 mM CTP	ParB(WT) 50 nM lambda DNA - 1 mM CTPγS
Number of values	44	55	22
Minimum	633.8	17.01	0.869
25% Percentile	1479	38.53	8.299
Median	1660	52.57	12.06
75% Percentile	2222	67.59	14.55
Maximum	3588	131.5	22.18
Range	2954	114.5	21.31
Mean	1805	53.85	11.87
Std. Deviation	563.6	20.98	5.293
Std. Error of Mean	84.97	2.829	1.129
Lower 95% CI of mean	1633	48.17	9.522
Upper 95% CI of mean	1976	59.52	14.22

	ParB(WT) 50 nM *parS* DNA - 0 mM CTP	ParB(WT) 50 nM *parS* DNA - 1 mM CTP	ParB(WT) 50 nM *parS* DNA - 1 mM CTPγS
Number of values	43	47	24
Minimum	468.8	20.35	4.008
25% Percentile	910.1	45.71	7.561
Median	1270	71.72	23.03
75% Percentile	1633	99.05	37.65
Maximum	2644	281.5	61.39
Range	2175	261.1	57.38
Mean	1321	80.44	26.07
Std. Deviation	508.8	53.22	18.04
Std. Error of Mean	77.59	7.763	3.682
Lower 95% CI of mean	1164	64.82	18.45
Upper 95% CI of mean	1477	96.07	33.68

Table 1., cont.

	ParB(KCK-WT) 50 nM lambda DNA - 0 mM CTP	ParB(KCK-WT) 50 nM lambda DNA - 1 mM CTP	ParB(KCK-WT) 50 nM lambda DNA - 1 mM CTPγS
Number of values	37	73	21
Minimum	379.9	53.31	107.1
25% Percentile	658	183.2	145.8
Median	1120	332.7	196.7
75% Percentile	1874	665	350.1
Maximum	2584	1496	583.1
Range	2205	1443	475.9
Mean	1298	489.1	250.9
Std. Deviation	628.6	391.4	134
Std. Error of Mean	103.3	45.81	29.23
Lower 95% CI of mean	1088	397.8	189.9
Upper 95% CI of mean	1507	580.4	311.8

	ParB(KCK-WT) 50 nM *parS* DNA - 0 mM CTP	ParB(KCK-WT) 50 nM *parS* DNA - 1 mM CTP	ParB(KCK-WT) 50 nM *parS* DNA - 1 mM CTPγS
Number of values	19	64	31
Minimum	1255	109.4	81.42
25% Percentile	1653	274.9	133.9
Median	1937	402.3	182.9
75% Percentile	2665	523.8	237
Maximum	3734	829.4	317.8
Range	2480	720	236.3
Mean	2152	398	178.7
Std. Deviation	660.1	166.9	62.79
Std. Error of Mean	151.4	20.86	11.28
Lower 95% CI of mean	1834	356.3	155.7
Upper 95% CI of mean	2470	439.7	201.7

Table 1., cont.

	ParB(WT-KCK) 50 nM lambda DNA - 0 mM CTP	ParB(WT-KCK) 50 nM lambda DNA - 1 mM CTP	ParB(WT-KCK) 50 nM lambda DNA - 1 mM CTPγS
Number of values	32	38	35
Minimum	789.8	238.9	3.353
25% Percentile	1112	293.6	14.78
Median	1744	334	22.48
75% Percentile	2037	367.2	26.56
Maximum	2780	468.6	40.97
Range	1990	229.8	37.62
Mean	1671	334.4	21.14
Std. Deviation	577.4	51.79	8.811
Std. Error of Mean	102.1	8.402	1.489
Lower 95% CI of mean	1462	317.4	18.12
Upper 95% CI of mean	1879	351.5	24.17

	ParB(WT-KCK) 50 nM *parS* DNA - 0 mM CTP	ParB(WT-KCK) 50 nM *parS* DNA - 1 mM CTP	ParB(WT-KCK) 50 nM *parS* DNA - 1 mM CTPγS
Number of values	59	37	31
Minimum	566.2	121.7	27
25% Percentile	1609	218.3	41.94
Median	1801	273	51.18
75% Percentile	2022	314.1	60.53
Maximum	2985	584.9	86.93
Range	2419	463.2	59.94
Mean	1798	277.2	52.01
Std. Deviation	398.9	88.85	15.1
Std. Error of Mean	51.93	14.61	2.712
Lower 95% CI of mean	1694	247.6	46.47
Upper 95% CI of mean	1902	306.8	57.55

Table 1., cont.

	ParB(WT) 30 nM lambda DNA - 0 mM CTP	ParB(WT) 30 nM lambda DNA - 1 mM CTP	ParB(WT) 30 nM lambda DNA - 1 mM CTPγS
Number of values	37	51	19
Minimum	444	0.9837	0.5425
25% Percentile	684.6	14.84	3.379
Median	1075	22.68	7.118
75% Percentile	1268	32.83	11.86
Maximum	2126	68.62	20.9
Range	1682	67.64	20.35
Mean	1019	23.51	7.983
Std. Deviation	370.9	13.54	5.986
Std. Error of Mean	60.97	1.896	1.373
Lower 95% CI of mean	895.5	19.7	5.098
Upper 95% CI of mean	1143	27.31	10.87

	ParB(WT) 30 nM *parS* DNA - 0 mM CTP	ParB(WT) 30 nM *parS* DNA - 1 mM CTP	ParB(WT) 30 nM *parS* DNA - 1 mM CTPγS
Number of values	39	34	19
Minimum	340.9	14.65	2.578
25% Percentile	500.7	21.39	19.94
Median	764.7	31.1	23.87
75% Percentile	893	57.7	35.58
Maximum	1253	133.5	77.51
Range	912.2	118.8	74.94
Mean	733.8	40.22	28.93
Std. Deviation	251	25.84	18.41
Std. Error of Mean	40.2	4.432	4.224
Lower 95% CI of mean	652.4	31.2	20.05
Upper 95% CI of mean	815.2	49.24	37.8

Table 1., cont.

	ParB(WT) 10 nM lambda DNA - 0 mM CTP	ParB(WT) 10 nM lambda DNA - 1 mM CTP	ParB(WT) 10 nM lambda DNA - 1 mM CTPγS
Number of values	38	39	7
Minimum	33.77	0.05774	0.02402
25% Percentile	66.84	0.961	0.4388
Median	74.98	1.32	0.8762
75% Percentile	82.44	1.786	2.036
Maximum	137.2	3.03	2.114
Range	103.4	2.972	2.09
Mean	77.69	1.405	1.098
Std. Deviation	19.03	0.6948	0.8349
Std. Error of Mean	3.086	0.1113	0.3156
Lower 95% CI of mean	71.43	1.179	0.3258
Upper 95% CI of mean	83.94	1.63	1.87

	ParB(WT) 10 nM *parS* DNA - 0 mM CTP	ParB(WT) 10 nM *parS* DNA - 1 mM CTP	ParB(WT) 10 nM *parS* DNA - 1 mM CTPγS
Number of values	41	28	14
Minimum	115.4	0.1119	0.7596
25% Percentile	142.6	0.4296	2.913
Median	156.1	2.47	4.815
75% Percentile	184.3	3.817	6.462
Maximum	333.7	11.09	9.393
Range	218.3	10.97	8.633
Mean	165.5	2.663	4.97
Std. Deviation	39.05	2.642	2.485
Std. Error of Mean	6.098	0.4993	0.6642
Lower 95% CI of mean	153.2	1.639	3.535
Upper 95% CI of mean	177.8	3.688	6.405

Table 2. Compaction rates in nm/sec for untagged and tagged ParB(WT), ParB(KCK-WT) and ParB(WT-KCK) on lambda DNA and *parS* DNA

	ParB(R80A) 50 nM – with Mg^{2+} lambda DNA - 0 mM CTP	ParB(R80A) 50 nM – with Mg^{2+} lambda DNA - 1 mM CTP	ParB(R80A) 50 nM – with Mg^{2+} lambda DNA - 1 mM CTPγS
Number of values	58	38	18
Minimum	33.59	23.54	2.537
25% Percentile	56.44	49.69	5.924
Median	73.76	76.87	9.12
75% Percentile	156	214.6	12.05
Maximum	243.8	583.7	24.23
Range	210.2	560.2	21.69
Mean	99.4	142.9	10.03
Std. Deviation	57.84	142.6	5.597
Std. Error of Mean	7.595	23.13	1.319
Lower 95% CI of mean	84.19	96.05	7.244
Upper 95% CI of mean	114.6	189.8	12.81

	ParB(R80A) 50 nM – no Mg^{2+} lambda DNA - 0 mM CTP	ParB(R80A) 50 nM – no Mg^{2+} lambda DNA - 1 mM CTP	ParB(R80A) 50 nM – no Mg^{2+} lambda DNA - 1 mM CTPγS
Number of values	52	34	27
Minimum	108.7	11.8	3.915
25% Percentile	359.3	17.38	7.848
Median	683.2	23.43	9.408
75% Percentile	880.9	33.81	11.53
Maximum	1509	70.2	26.6
Range	1401	58.41	22.68
Mean	672.8	26.05	10.74
Std. Deviation	361.5	11.87	5.71
Std. Error of Mean	50.13	2.036	1.099
Lower 95% CI of mean	572.2	21.91	8.478
Upper 95% CI of mean	773.4	30.19	13

Table 2, cont.

	ParB(R80A) 50 nM – with Mg^{2+} *parS* DNA - 0 mM CTP	ParB(R80A) 50 nM – with Mg^{2+} *parS* DNA - 1 mM CTP	ParB(R80A) 50 nM – with Mg^{2+} *parS* DNA - 1 mM CTPγS
Number of values	44	38	28
Minimum	35.47	25.11	0.5385
25% Percentile	49.19	45.33	2.373
Median	57.7	124.3	5.055
75% Percentile	217.1	164.6	6.601
Maximum	316	478.7	13.51
Range	280.5	453.6	12.97
Mean	108.4	132.2	5.209
Std. Deviation	88.06	94.95	3.345
Std. Error of Mean	13.28	15.4	0.6322
Lower 95% CI of mean	81.6	101	3.911
Upper 95% CI of mean	135.1	163.4	6.506

	ParB(R80A) 50 nM – no Mg^{2+} *parS* DNA - 0 mM CTP	ParB(R80A) 50 nM – no Mg^{2+} *parS* DNA - 1 mM CTP	ParB(R80A) 50 nM – no Mg^{2+} *parS* DNA - 1 mM CTPγS
Number of values	42	57	16
Minimum	114.7	4.113	5.895
25% Percentile	405.7	13.11	6.74
Median	754.1	22.08	9.671
75% Percentile	1078	30.09	11.65
Maximum	1512	68.91	17.88
Range	1398	64.8	11.99
Mean	760.4	22.96	9.692
Std. Deviation	390	12.55	3.354
Std. Error of Mean	60.18	1.663	0.8384
Lower 95% CI of mean	638.9	19.63	7.905
Upper 95% CI of mean	882	26.29	11.48

Table 2, cont.

	ParB(KCK-R80A) 50 nM - with Mg^{2+} lambda DNA - 0 mM CTP	ParB(KCK-R80A) 50 nM - with Mg^{2+} lambda DNA 1 mM CTP	ParB(KCK-R80A) 50 nM - with Mg^{2+} lambda DNA - 1 mM CTPγS
Number of values	53	26	22
Minimum	303.7	233.5	298.2
25% Percentile	488.3	334.7	483
Median	585	411.2	625.6
75% Percentile	706	481.5	849.8
Maximum	1040	898.4	1929
Range	736.3	664.9	1631
Mean	600	431.2	746
Std. Deviation	160.3	144.9	376.6
Std. Error of Mean	22.02	28.41	80.3
Lower 95% CI of mean	555.8	372.7	579
Upper 95% CI of mean	644.2	489.7	913

	ParB(KCK-R80A) 50 nM - with Mg^{2+} *parS* DNA - 0 mM CTP	ParB(KCK-R80A) 50 nM - with Mg^{2+} *parS* DNA - 1 mM CTP	ParB(KCK-R80A) 50 nM - with Mg^{2+} *parS* DNA - 1 mM CTPγS
Number of values	26	23	30
Minimum	631.4	441.2	191
25% Percentile	884.3	567.2	296.2
Median	992	685.7	483.4
75% Percentile	1300	2108	647.9
Maximum	1991	2790	958.9
Range	1359	2349	767.9
Mean	1112	1243	479.5
Std. Deviation	314.3	836.7	197.2
Std. Error of Mean	61.64	174.5	36
Lower 95% CI of mean	985.5	881.3	405.8
Upper 95% CI of mean	1239	1605	553.1

Table 2, cont.

	ParB(R80A-KCK) 50 nM - with Mg^{2+} lambda DNA - 0 mM CTP	ParB(R80A-KCK) 50 nM - with Mg^{2+} lambda DNA 1 mM CTP	ParB(R80A-KCK) 50 nM - with Mg^{2+} lambda DNA - 1 mM CTPγS
Number of values	43	29	29
Minimum	253.9	403.5	224.1
25% Percentile	367.3	553.6	297.3
Median	564.7	600	667.2
75% Percentile	945.5	769.9	863.8
Maximum	1695	1355	1854
Range	1441	951.2	1629
Mean	677.8	677.3	674.3
Std. Deviation	378.6	219.4	387.2
Std. Error of Mean	57.74	40.74	71.91
Lower 95% CI of mean	561.3	593.9	527
Upper 95% CI of mean	794.4	760.8	821.6

	ParB(R80A-KCK) 50 nM - with Mg^{2+} *parS* DNA - 0 mM CTP	ParB(R80A-KCK) 50 nM - with Mg^{2+} *parS* DNA - 1 mM CTP	ParB(R80A-KCK) 50 nM - with Mg^{2+} *parS* DNA - 1 mM CTPγS
Number of values	40	35	38
Minimum	242.8	160.3	32.59
25% Percentile	571	324.1	55.73
Median	728.7	713	76.57
75% Percentile	967.9	755.4	95.51
Maximum	1455	1971	131.3
Range	1212	1811	98.69
Mean	785.1	615.9	77.96
Std. Deviation	274.7	337.9	25.18
Std. Error of Mean	43.43	57.11	4.085
Lower 95% CI of mean	697.2	499.8	69.69
Upper 95% CI of mean	872.9	732	86.24

Table 3. Unpaired t-test table for statistics with two-tailed p-values for ParB(WT)

Column "B" vs. Column "A"	WT50-parS-0mMCTP vs. WT50-lambda-0mMCTP	KCK-WT50 parS 0mMCTP vs. KCK-WT50 lambda 0mMCTP	WT50-KCK parS 0mMCTP vs. WT50-KCK lambda 0mMCTP	KCK-WT50 lambda 0mMCTP vs. WT50-lambda-0mMCTP	WT50-KCK lambda 0mMCTP vs. WT50-lambda-0mMCTP	WT50-KCK lambda 0mMCTP vs. KCK-WT50 lambda 0mMCTP	KCK-WT50 parS 0mMCTP vs. WT50-parS-0mMCTP	WT50-KCK parS 0mMCTP vs. WT50-parS-0mMCTP	WT50-KCK parS 0mMCTP vs. KCK-WT50 parS 0mMCTP
P value	<0.0001	<0.0001	0.2202	0.0003	0.3138	0.0131	<0.0001	<0.0001	0.0059
P value summary	****	****	ns	***	ns	*	****	****	**
(P < 0.05)?	Yes	Yes	No	Yes	No	Yes	Yes	Yes	Yes
t, df	t=4.200, df=85	t=4.734, df=54	t=1.235, df=89	t=3.825, df=79	t=1.014, df=74	t=2.550, df=67	t=5.401, df=60	t=5.304, df=100	t=2.834, df=76
Mean column A	1805	1298	1671	1805	1805	1298	1321	1321	2152
Mean column B	1321	2152	1798	1298	1671	1671	2152	1798	1798
Difference between means (B - A) ± SEM	-483.8 ± 115.2	854.1 ± 180.4	127.1 ± 102.9	-506.9 ± 132.5	-134.2 ± 132.3	372.7 ± 146.2	831.0 ± 153.9	476.8 ± 89.89	-354.3 ± 125.0
95% confidence interval	-712.9 to -254.8	492.4 to 1216	-77.43 to 331.6	-770.7 to -243.1	-397.8 to 129.4	80.97 to 664.4	523.3 to 1139	298.4 to 655.1	-603.3 to -105.3
R squared (eta squared)	0.1719	0.2933	0.01684	0.1563	0.01371	0.08847	0.3272	0.2195	0.09557
Sample size A	44	37	32	44	44	37	43	43	19
Sample size B	43	19	59	37	32	32	19	59	59

Table 3, cont.

Column "B"	WT50-parS-1mMCTP	KCK-WT50 parS 1mMCTP	WT50-KCK parS 1mMCTP	KCK-WT50 lambda 1mMCTP	WT50-KCK lambda 1mMCTP	WT50-KCK lambda 1mMCTP	KCK-WT50 parS 1mMCTP	WT50-KCK parS 1mMCTP	WT50-KCK parS 1mMCTP
	vs.	vs.	vs.	vs.	vs.	vs.	vs.	vs.	vs.
Column "A"	WT50-lambda-1mMCTP	KCK-WT50 lambda 1mMCTP	WT50-KCK lambda 1mMCTP	WT50-lambda-1mMCTP	WT50-lambda-1mMCTP	KCK-WT50 lambda 1mMCTP	WT50-parS-1mMCTP	WT50-parS-1mMCTP	KCK-WT50 parS 1mMCTP
P value	0.0009	0.0861	0.001	<0.0001	<0.0001	0.0172	<0.0001	<0.0001	<0.0001
P value summary	***	ns	**	****	****	*	****	****	****
(P < 0.05)?	Yes	No	Yes	Yes	Yes	Yes	Yes	Yes	Yes
t, df	t=3.411, df=100	t=1.729, df=135	t=3.421, df=73	t=8.231, df=126	t=36.18, df=91	t=2.420, df=109	t=12.57, df=109	t=12.59, df=82	t=4.076, df=99
Mean column A	53.85	489.1	334.4	53.85	53.85	489.1	80.44	80.44	398
Mean column B	80.44	398	277.2	489.1	334.4	334.4	398	277.2	277.2
Difference between means (B - A) ± SEM	26.60 ± 7.797	-91.11 ± 52.69	-57.26 ± 16.74	435.2 ± 52.88	280.6 ± 7.756	-154.7 ± 63.91	317.5 ± 25.26	196.7 ± 15.63	-120.8 ± 29.64
95% confidence interval	11.13 to 42.07	-195.3 to 13.10	-90.62 to -23.90	330.6 to 539.9	265.2 to 296.0	-281.3 to -27.98	267.5 to 367.6	165.7 to 227.8	-179.6 to -62.00
R squared (eta squared)	0.1042	0.02167	0.1381	0.3497	0.935	0.05098	0.5918	0.6591	0.1437
Sample size A	55	73	38	55	55	73	47	47	64
Sample size B	47	64	37	73	38	38	64	37	37

Table 3, cont.

Column "B"	WT50-parS-1mMCTPγS	KCK-WT50 parS 1mMCTPγS	WT50-KCK parS 1mMCTPγS	KCK-WT50 lambda 1mMCTPγS	WT50-KCK lambda 1mMCTPγS	WT50-KCK lambda 1mMCTPγS	KCK-WT50 parS 1mMCTPγS	WT50-KCK parS 1mMCTPγS	WT50-KCK parS 1mMCTPγS
vs.	vs.	vs.	vs.	vs.	vs.	vs.	vs.	vs.	vs.
Column "A"	WT50-lambda-1mMCTPγS	KCK-WT50 lambda 1mMCTPγS	WT50-KCK lambda 1mMCTPγS	WT50-lambda-1mMCTPγS	WT50-lambda-1mMCTPγS	KCK-WT50 lambda 1mMCTPγS	WT50-parS-1mMCTPγS	WT50-parS-1mMCTPγS	KCK-WT50 lambda 1mMCTPγS
P value	0.0009	0.0118	<0.0001	<0.0001	<0.0001	<0.0001	<0.0001	<0.0001	<0.0001
P value summary (P < 0.05)?	***	*	****	****	****	****	****	****	****
	Yes	Yes	Yes	Yes	Yes	Yes	Yes	Yes	Yes
t, df	t=3.552, df=44	t=2.614, df=50	t=10.28, df=64	t=8.367, df=41	t=4.449, df=55	t=10.17, df=54	t=11.52, df=53	t=5.804, df=53	t=8.227, df=50
Mean column A	11.87	250.9	21.14	11.87	11.87	250.9	26.07	26.07	250.9
Mean column B	26.07	178.7	52.01	250.9	21.14	21.14	178.7	52.01	52.01
Difference between means (B - A) ± SEM	14.20 ± 3.998	-72.17 ± 27.61	30.87 ± 3.002	239.0 ± 28.57	9.274 ± 2.084	-229.7 ± 22.58	152.6 ± 13.24	25.94 ± 4.470	-198.9 ± 24.17
95% confidence interval	6.142 to 22.26	-127.6 to -16.72	24.87 to 36.87	181.3 to 296.7	5.097 to 13.45	-275.0 to -184.4	126.1 to 179.2	16.98 to 34.91	-247.4 to -150.3
R squared (eta squared)	0.2228	0.1202	0.623	0.6306	0.2647	0.6571	0.7147	0.3886	0.5751
Sample size A	22	21	35	22	22	21	24	24	21
Sample size B	24	31	31	21	35	35	31	31	31

Table 3, cont.

Column "B"	WT50-lambda-1mMCTP vs.	WT50-lambda-1mMCTPγS vs.	WT50-parS-1mMCTP vs.	WT50-parS-1mMCTPγS vs.	KCK-WT50 lambda 1mMCTP vs.	KCK-WT50 lambda 1mMCTPγS vs.
Column "A"	WT50-lambda-0mMCTP	WT50-lambda-1mMCTP	WT50-parS-0mMCTP	WT50-parS-1mMCTP	KCK-WT50 lambda 0mMCTP	KCK-WT50 lambda 1mMCTP
P value	<0.0001	<0.0001	<0.0001	<0.0001	<0.0001	0.0075
P value summary	****	****	****	****	****	**
(P < 0.05)?	Yes	Yes	Yes	Yes	Yes	Yes
t, df	t=23.05, df=97	t=9.234, df=75	t=16.62, df=88	t=4.850, df=69	t=8.288, df=108	t=2.734, df=92
Mean column A	1805	53.85	1321	80.44	1298	489.1
Mean column B	53.85	11.87	80.44	26.07	489.1	250.9
Difference between means (B - A) ± SEM	-1751 ± 75.97	-41.98 ± 4.546	-1240 ± 74.62	-54.38 ± 11.21	-808.7 ± 97.58	-238.2 ± 87.12
95% confidence interval	-1902 to -1600	-51.03 to -32.92	-1389 to -1092	-76.74 to -32.01	-1002 to -615.3	-411.2 to -65.20
R squared (eta squared)	0.8456	0.532	0.7585	0.2542	0.3888	0.07517
Sample size A	44	55	43	47	37	73
Sample size B	55	22	47	24	73	21

Table 3, cont.

Column "B"	KCK-WT50 parS 1mMCTP	KCK-WT50 parS 1mMCTPγS	WT50-KCK lambda 1mMCTP	WT50-KCK lambda 1mMCTPγS	WT50-KCK parS 1mMCTP	WT50-KCK parS 1mMCTPγS
	vs.	vs.	vs.	vs.	vs.	vs.
Column "A"	KCK-WT50 parS 0mMCTP	KCK-WT50 parS 1mMCTP	WT50-KCK lambda 0mMCTP	WT50-KCK lambda 1mMCTP	WT50-KCK parS 0mMCTP	WT50-KCK parS 1mMCTP
P value	<0.0001	<0.0001	<0.0001	<0.0001	<0.0001	<0.0001
P value summary (P < 0.05)?	****	****	****	****	****	****
	Yes	Yes	Yes	Yes	Yes	Yes
t, df	t=19.50, df=81	t=7.062, df=93	t=14.21, df=68	t=35.30, df=71	t=22.79, df=94	t=13.93, df=66
Mean column A	2152	398	1671	334.4	1798	277.2
Mean column B	398	178.7	334.4	21.14	277.2	52.01
Difference between means (B - A) ± SEM	-1754 ± 89.93	-219.3 ± 31.05	-1336 ± 93.99	-313.3 ± 8.875	-1520 ± 66.71	-225.2 ± 16.17
95% confidence interval	-1933 to -1575	-280.9 to -157.6	-1524 to -1149	-331.0 to -295.6	-1653 to -1388	-257.5 to -192.9
R squared (eta squared)	0.8244	0.3491	0.7482	0.9461	0.8468	0.7461
Sample size A	19	64	32	38	59	37
Sample size B	64	31	38	35	37	31

Table 3, cont.

Column "B"	WT30-lambda-0mMCTP vs.	WT10-lambda-0mMCTP vs.	WT30-parS-0mMCTP vs.	WT10-parS-0mMCTP vs.	WT30-lambda-1mMCTP vs.	WT10-lambda-1mMCTP vs.
Column "A"	WT50-lambda-0mMCTP	WT30-lambda-0mMCTP	WT50-parS-0mMCTP	WT30-parS-0mMCTP	WT50-lambda-1mMCTP	WT30-lambda-1mMCTP
P value	<0.0001	<0.0001	<0.0001	<0.0001	<0.0001	<0.0001
P value summary	****	****	****	****	****	****
(P < 0.05)?	Yes	Yes	Yes	Yes	Yes	Yes
t, df	t=7.256, df=79	t=15.63, df=73	t=6.520, df=80	t=14.32, df=78	t=8.770, df=104	t=10.17, df=88
Mean column A	1805	1019	1321	733.8	53.85	23.51
Mean column B	1019	77.69	733.8	165.5	23.51	1.405
Difference between means (B - A) ± SEM	-785.6 ± 108.3	-941.4 ± 60.23	-587.1 ± 90.05	-568.3 ± 39.69	-30.34 ± 3.459	-22.10 ± 2.173
95% confidence interval	-1001 to -570.1	-1061 to -821.4	-766.3 to -407.9	-647.3 to -489.3	-37.20 to -23.48	-26.42 to -17.78
R squared (eta squared)	0.3999	0.7699	0.347	0.7244	0.4251	0.5403
Sample size A	44	37	43	39	55	51
Sample size B	37	38	39	41	51	39

Table 3, cont.

Column "B"	WT30-parS-1mMCTP	WT10-parS-1mMCTP	WT30-lambda-1mMCTPγS	WT10-lambda-1mMCTPγS	WT30-parS-1mMCTPγS	WT10-parS-1mMCTPγS
Column "A"	WT50-parS-1mMCTP	WT30-parS-1mMCTP	WT50-lambda-1mMCTPγS	WT30-lambda-1mMCTPγS	WT50-parS-1mMCTPγS	WT30-parS-1mMCTPγS
P value	0.0001	<0.0001	0.0333	0.0063	0.6118	<0.0001
P value summary (P < 0.05)?	***	****	*	**	ns	****
t, df	Yes t=4.069, df=79	Yes t=7.646, df=60	Yes t=2.207, df=39	Yes t=2.994, df=24	No t=0.5113, df=41	Yes t=4.816, df=31
Mean column A	80.44	40.22	11.87	7.983	26.07	28.93
Mean column B	40.22	2.663	7.983	1.098	28.93	4.97
Difference between means (B - A) ± SEM	-40.23 ± 9.887	-37.55 ± 4.912	-3.886 ± 1.761	-6.885 ± 2.300	2.858 ± 5.590	-23.96 ± 4.974
95% confidence interval	-59.90 to -20.55	-47.38 to -27.73	-7.449 to -0.3239	-11.63 to -2.139	-8.430 to 14.15	-34.10 to -13.81
R squared (eta squared)	0.1732	0.4935	0.111	0.2719	0.006337	0.428
Sample size A	47	34	22	19	24	19
Sample size B	34	28	19	7	19	14

Table 4. Unpaired t-test table for statistics with two-tailed p-values for ParB(R80A)

Column "B" vs. Column "A"	R80A-50 Mg2+ parS 0mM CTP vs. R80A-50 Mg2+ lambda 0mM CTP	KCK-R80A-50 Mg2+ parS 0mM CTP vs. KCK-R80A-50 Mg2+ lambda 0mM CTP	R80A50-KCK Mg2+ parS 0mM CTP vs. R80A50-KCK Mg2+ lambda 0mM CTP	KCK-R80A-50 Mg2+ lambda 0mM CTP vs. R80A-50 Mg2+ lambda 0mM CTP	R80A50-KCK Mg2+ lambda 0mM CTP vs. R80A-50 Mg2+ lambda 0mM CTP	R80A50-KCK Mg2+ lambda 0mM CTP vs. KCK-R80A-50 Mg2+ lambda 0mM CTP	KCK-R80A-50 Mg2+ parS 0mM CTP vs. R80A-50 Mg2+ parS 0mM CTP	R80A50-KCK Mg2+ parS 0mM CTP vs. R80A-50 Mg2+ parS 0mM CTP	R80A50-KCK Mg2+ parS 0mM CTP vs. KCK-R80A-50 Mg2+ parS 0mM CTP
P value	0.5367	<0.0001	0.1462	<0.0001	<0.0001	0.1784	<0.0001	<0.0001	<0.0001
P value summary	ns	****	ns	****	****	ns	****	****	****
(P < 0.05)?	No	Yes	No	Yes	Yes	No	Yes	Yes	Yes
t, df	t=0.6200, df=100	t=9.626, df=77	t=1.467, df=81	t=22.26, df=109	t=11.48, df=99	t=1.356, df=94	t=19.99, df=68	t=15.50, df=82	t=4.469, df=64
Mean column A	99.4	600	677.8	99.4	99.4	600	108.4	108.4	1112
Mean column B	108.4	1112	785.1	600	677.8	677.8	1112	785.1	785.1
Difference between means (B - A) ± SEM	8.973 ± 14.47	512.4 ± 53.23	107.2 ± 73.07	500.6 ± 22.49	578.5 ± 50.41	77.84 ± 57.42	1004 ± 50.23	676.7 ± 43.67	-327.4 ± 73.26
95% confidence interval	-19.74 to 37.69	406.4 to 618.4	-38.19 to 252.6	456.0 to 545.2	478.4 to 678.5	-36.16 to 191.8	903.8 to 1104	589.8 to 763.5	-473.7 to -181.0
R squared (eta squared)	0.003829	0.5462	0.02588	0.8197	0.5709	0.01918	0.8546	0.7455	0.2378
Sample size A	58	53	43	58	58	53	44	44	26
Sample size B	44	26	40	53	43	43	26	40	40

Table 4, cont.

Column "B" vs. Column "A"	R80A-50 Mg2+ parS +K1:S271mM CTP vs. R80A-50 Mg2+ lambda 1mM CTP	KCK-R80A-50 Mg2+ parS 1mM CTP vs. KCK-R80A-50 Mg2+ lambda 1mM CTP	R80A50-KCK Mg2+ parS 1mM CTP vs. R80A50-KCK Mg2+ lambda 1mM CTP	KCK-R80A-50 Mg2+ lambda 1mM CTP vs. R80A-50 Mg2+ lambda 1mM CTP	R80A50-KCK Mg2+ lambda 1mM CTP vs. R80A-50 Mg2+ lambda 1mM CTP	R80A50-KCK Mg2+ lambda 1mM CTP vs. KCK-R80A-50 Mg2+ lambda 1mM CTP	KCK-R80A-50 Mg2+ parS 1mM CTP vs. R80A-50 Mg2+ parS 1mM CTP	R80A50-KCK Mg2+ parS 1mM CTP vs. R80A-50 Mg2+ parS 1mM CTP	R80A50-KCK Mg2+ parS 1mM CTP vs. KCK-R80A-50 Mg2+ parS 1mM CTP
P value	0.7016	<0.0001	0.4029	<0.0001	<0.0001	<0.0001	<0.0001	<0.0001	0.0002
P value summary	ns	****	ns	****	****	****	****	****	***
(P < 0.05)?	No	Yes	No	Yes	Yes	Yes	Yes	Yes	Yes
t, df	t=0.3846, df=74	t=4.873, df=47	t=0.8422, df=62	t=7.893, df=62	t=12.06, df=65	t=4.849, df=53	t=8.142, df=59	t=8.473, df=71	t=3.982, df=56
Mean column A	142.9	431.2	677.3	142.9	142.9	431.2	132.2	132.2	1243
Mean column B	132.2	1243	615.9	431.2	677.3	677.3	1243	615.9	615.9
Difference between means (B - A) ± SEM	-10.69 ± 27.79	812.0 ± 166.6	-61.42 ± 72.93	288.3 ± 36.52	534.4 ± 44.32	246.1 ± 50.76	1111 ± 136.4	483.7 ± 57.08	-627.3 ± 157.5
95% confidence interval	-66.06 to 44.68	476.8 to 1147	-207.2 to 84.36	215.3 to 361.3	445.9 to 622.9	144.3 to 347.9	837.9 to 1384	369.9 to 597.5	-942.8 to -311.7
R squared (eta squared)	0.001995	0.3356	0.01131	0.5012	0.6911	0.3073	0.5291	0.5028	0.2207
Sample size A	38	26	29	38	38	26	38	38	23
Sample size B	38	23	35	26	29	29	23	35	35

Table 4, cont.

Column "B" vs. Column "A"	R80A-50 Mg2+ parS 1mM CTPγS vs. R80A-50 Mg2+ lambda 1mM CTPγS	KCK-R80A-50 Mg2+ parS 1mM CTPγS vs. KCK-R80A-50 Mg2+ lambda 1mM CTPγS	R80A50-KCK Mg2+ parS 1mM CTPγS vs. R80A50-KCK Mg2+ lambda 1mM CTPγS	KCK-R80A-50 Mg2+ lambda 1mM CTPγS vs. R80A-50 Mg2+ lambda 1mM CTPγS	R80A50-KCK Mg2+ lambda 1mM CTPγS vs. R80A-50 Mg2+ lambda 1mM CTPγS	R80A50-KCK Mg2+ lambda 1mM CTPγS vs. KCK-R80A-50 Mg2+ lambda 1mM CTPγS	KCK-R80A-50 Mg2+ parS 1mM CTPγS vs. R80A-50 Mg2+ parS 1mM CTPγS	R80A50-KCK Mg2+ parS 1mM CTPγS vs. R80A-50 Mg2+ parS 1mM CTPγS	R80A50-KCK Mg2+ parS 1mM CTPγS vs. KCK-R80A-50 Mg2+ parS 1mM CTPγS
P value	0.0007	0.0017	<0.0001	<0.0001	<0.0001	0.5108	<0.0001	<0.0001	<0.0001
P value summary	***	**	****	****	****	ns	****	****	****
(P < 0.05)?	Yes	Yes	Yes	Yes	Yes	No	Yes	Yes	Yes
t, df	t=3.662, df=44	t=3.313, df=50	t=9.490, df=65	t=8.270, df=38	t=7.247, df=45	t=0.6624, df=49	t=12.72, df=56	t=15.16, df=64	t=12.45, df=66
Mean column A	10.03	746	674.3	10.03	10.03	746	5.209	5.209	479.5
Mean column B	5.209	479.5	77.96	746	674.3	674.3	479.5	77.96	77.96
Difference between means (B - A) ± SEM	-4.819 ± 1.316	-266.5 ± 80.44	-596.3 ± 62.84	735.9 ± 88.99	664.3 ± 91.66	-71.68 ± 108.2	474.2 ± 37.29	72.75 ± 4.799	-401.5 ± 32.25
95% confidence interval	-7.471 to -2.167	-428.1 to -105.0	-721.8 to -470.8	555.8 to 916.1	479.7 to 848.9	-289.1 to 145.8	399.6 to 548.9	63.17 to 82.34	-465.9 to -337.1
Sample size A	18	22	29	18	18	22	28	28	30
Sample size B	28	30	38	22	29	29	30	38	38

Table 4, cont.

Column "B" vs. Column "A"	R80A-50 Mg2+ lambda 1mM CTP vs. R80A-50 Mg2+ lambda 0mM CTP	R80A-50 Mg2+ lambda 1mM CTPγS vs. R80A-50 Mg2+ lambda 1mM CTP	R80A-50 Mg2+ lambda 1mM CTPγS vs. R80A-50 Mg2+ lambda 0mM CTP	R80A-50 Mg2+ parS 1mM CTP vs. R80A-50 Mg2+ parS 0mM CTP	R80A-50 Mg2+ parS 1mM CTPγS vs. R80A-50 Mg2+ parS 1mM CTP	R80A-50 Mg2+ parS 1mM CTPγS vs. R80A-50 Mg2+ parS 0mM CTP	KCK-R80A-50 Mg2+ lambda 1mM CTP vs. KCK-R80A-50 Mg2+ lambda 0mM CTP	KCK-R80A-50 Mg2+ lambda 1mM CTPγS vs. KCK-R80A-50 Mg2+ lambda 1mM CTP	KCK-R80A-50 Mg2+ lambda 1mM CTPγS vs. KCK-R80A-50 Mg2+ lambda 0mM CTP
P value	0.0401	0.0002	<0.0001	0.2416	<0.0001	<0.0001	<0.0001	0.0003	0.0206
P value summary	*	***	****	ns	****	****	****	***	*
(P < 0.05)?	Yes	Yes	Yes	No	Yes	Yes	Yes	Yes	Yes
t, df	t=2.082, df=94	t=3.934, df=54	t=6.516, df=74	t=1.180, df=80	t=7.061, df=64	t=6.180, df=70	t=4.536, df=77	t=3.937, df=46	t=2.367, df=73
Mean column A	99.4	142.9	99.4	108.4	132.2	108.4	600	431.2	600
Mean column B	142.9	10.03	10.03	132.2	5.209	5.209	431.2	746	746
Difference between means (B - A) ± SEM	43.52 ± 20.90	-132.9 ± 33.78	-89.37 ± 13.72	23.86 ± 20.22	-127.0 ± 17.99	-103.2 ± 16.69	-168.8 ± 37.22	314.8 ± 79.95	146.0 ± 61.66
95% confidence interval	2.018 to 85.02	-200.6 to -65.16	-116.7 to -62.04	-16.38 to 64.10	-163.0 to -91.09	-136.5 to -69.87	-242.9 to -94.70	153.9 to 475.7	23.07 to 268.9
R squared (eta squared)	0.04408	0.2228	0.3646	0.0171	0.4379	0.353	0.2108	0.2521	0.07129
Sample size A	58	38	58	44	38	44	53	26	53
Sample size B	38	18	18	38	28	28	26	22	22

Table 4, cont.

Column "B" vs. Column "A"	KCK-R80A-50 Mg2+ parS 1mM CTP vs. KCK-R80A-50 Mg2+ parS 0mM CTP	KCK-R80A-50 Mg2+ parS 1mM CTPγS vs. KCK-R80A-50 Mg2+ parS 1mM CTP	KCK-R80A-50 Mg2+ parS 1mM CTPγS vs. KCK-R80A-50 Mg2+ parS 0mM CTP	R80A50-KCK Mg2+ lambda 1mM CTP vs. R80A50-KCK Mg2+ lambda 0mM CTP	R80A50-KCK Mg2+ lambda 1mM CTPγS vs. R80A50-KCK Mg2+ lambda 1mM CTP	R80A50-KCK Mg2+ lambda 1mM CTPγS vs. R80A50-KCK Mg2+ lambda 0mM CTP	R80A50-KCK Mg2+ parS 1mM CTP vs. R80A50-KCK Mg2+ parS 0mM CTP	R80A50-KCK Mg2+ parS 1mM CTPγS vs. R80A50-KCK Mg2+ parS 1mM CTP	R80A50-KCK Mg2+ parS 1mM CTPγS vs. R80A50-KCK Mg2+ parS 0mM CTP
P value	0.4626	<0.0001	<0.0001	0.9946	0.9709	0.9693	0.0194	<0.0001	<0.0001
P value summary (P < 0.05)?	ns No	**** Yes	**** Yes	ns No	ns No	ns No	* Yes	**** Yes	**** Yes
t, df	t=0.7407, df=47	t=4.840, df=51	t=9.153, df=54	t=0.006753, df=70	t=0.03660, df=56	t=0.03868, df=70	t=2.390, df=73	t=9.790, df=71	t=15.80, df=76
Mean column A	1112	1243	1112	677.8	677.3	677.8	785.1	615.9	785.1
Mean column B	1243	479.5	479.5	677.3	674.3	674.3	615.9	77.96	77.96
Difference between means (B - A) ± SEM	130.7 ± 176.5	-763.7 ± 157.8	-633.0 ± 69.16	-0.5265 ± 77.96	-3.025 ± 82.64	-3.551 ± 91.81	-169.1 ± 70.77	-537.9 ± 54.95	-707.1 ± 44.75
95% confidence interval	-224.4 to 485.9	-1080 to -447.0	-771.6 to -494.3	-156.0 to 155.0	-168.6 to 162.5	-186.7 to 179.6	-310.2 to -28.11	-647.5 to -428.4	-796.2 to -618.0
R squared (eta squared)	0.01154	0.3148	0.6081	6.515E-07	0.00002392	0.00002137	0.07258	0.5745	0.7666
Sample size A	26	23	26	43	29	43	40	35	40
Sample size B	23	30	30	29	29	29	35	38	38

Table 4, cont.

Column "B" vs. Column "A"	R80A-50 noMg2+ lambda 0mM CTP vs. R80A-50 Mg2+ lambda 0mM CTP	R80A-50 noMg2+ parS 0mM CTP vs. R80A-50 Mg2+ parS 0mM CTP	R80A-50 noMg2+ lambda 1mM CTP vs. R80A-50 Mg2+ lambda 1mM CTP	R80A-50 noMg2+ parS 1mM CTP vs. R80A-50 Mg2+ parS 1mM CTP	R80A-50 noMg2+ lambda 1mM CTPγS vs. R80A-50 Mg2+ lambda 1mM CTPγS	R80A-50 noMg2+ parS 1mM CTPγS vs. R80A-50 Mg2+ parS 1mM CTPγS	R80A-50 noMg2+ parS 0mM CTP vs. R80A-50 noMg2+ lambda 0mM CTP	R80A-50 noMg2+ parS 1mM CTP vs. R80A-50 noMg2+ lambda 1mM CTP	R80A-50 noMg2+ parS 1mM CTPγS vs. R80A-50 noMg2+ lambda 1mM CTPγS
P value	<0.0001	<0.0001	<0.0001	<0.0001	0.6829	0.0001	0.2622	0.2507	0.5097
P value summary	****	****	****	****	ns	***	ns	ns	ns
(P < 0.05)?	Yes	Yes	Yes	Yes	No	Yes	No	No	No
t, df	t=11.92, df=108	t=10.81, df=84	t=4.761, df=70	t=8.599, df=93	t=0.4113, df=43	t=4.272, df=42	t=1.128, df=92	t=1.156, df=89	t=0.6652, df=41
Mean column A	99.4	108.4	142.9	132.2	10.03	5.209	672.8	26.05	10.74
Mean column B	672.8	760.4	26.05	22.96	10.74	9.692	760.4	22.96	9.692
Difference between means (B - A) ± SEM	573.4 ± 48.12	652.1 ± 60.33	-116.9 ± 24.54	-109.3 ± 12.71	0.7091 ± 1.724	4.483 ± 1.049	87.65 ± 77.69	-3.082 ± 2.666	-1.045 ± 1.571
95% confidence interval	478.0 to 668.8	532.1 to 772.0	-165.8 to -67.92	-134.5 to -84.03	-2.768 to 4.186	2.365 to 6.601	-66.65 to 241.9	-8.380 to 2.215	-4.218 to 2.128
R squared (eta squared)	0.568	0.5817	0.2446	0.4429	0.003919	0.3029	0.01365	0.0148	0.01068
Sample size A	58	44	38	38	18	28	52	34	27
Sample size B	52	42	34	57	27	16	42	57	16

BIOGRAPHICAL SKETCH

Miranda Molina has completed her Master of Science degree while attending The University of Texas Rio Grande Valley in May of 2022. She attended and graduated from high school at James “Nikki” Rowe High School in May 2014 and went off to attend Texas A&M University to earn her Bachelor of Science degree in Biomedical Science in May 2018. After completing her master’s degree, Miranda hopes to attend medical school in the state of Texas to pursue her dream of being a physician and researcher.

Miranda can be contacted at mlmolina18@outlook.com for email correspondence, and for physical correspondence she can be reached at 3000 Wisteria Ave, McAllen, TX, zip code 78504.